MDA5 detects long polyI:C or dsRNA, whereas RIG-I detects short dsRNA or the 5′-triphosphate end of RNA generated by viral polymerases [47, 48], indicating that these RNA helicases have different roles in the detection of viruses. Which of these pathways predominantly senses virus species is under examination. The simple interpretation that MDA5 is required for the recognition of picornaviruses and RIG-I recognizes that dsRNA-forming viruses [49] may be amended following the analysis of many virus species.

Mf, mDC, and fibroblast cells derived from RIG-I- or MDA5-deficient mice still displayed type I IFN induction in response to polyI:C stimulation, and the production of type I IFN was still observed in pDCs derived from IPS-1–/– mice [50, 51]. However, it is notable that the 2 pathways in the TLR system and the cytoplasmic IPS-1 pathway are required for dsRNA responses in different situations and cell types [50, 52]. Collectively, these observations indicate that the various modes of the RNA pattern-sensing system cooperate to detect cytoplasmic virus replication in a variety of tissues/organs.

NK Cell Activation via the TLR2/MyD88 Pathway in Mf and mDC

In vitro stimulation of mouse mDC or Mf with TLR2 stimulators BCG-CWS (cell wall skeleton) or Pam2 lipopeptide causes these cells to become NK activation inducers [24, 53]. Both TLR2 and MyD88 are indispensable for this type of NK cell activation. At least in in vitro studies, MyD88–/– Mf fail to reciprocally activate NK cells via cell-cell contact [54]. Mf MyD88 signaling through TLRs is reported to induce expression of the NKG2D ligand retinoic acid early induced transcript (RAE)-1 [55]. NK cells are then activated by MyD88-stimulated Mf. The NKG2D receptor on NK cells is downregulated by the RAE-1-NKG2D interaction [55]. MyD88 can be activated via the inflammasome pathway in human Mf [56] without the participation of TLR2. IL-1β or IL-18 (or possibly IL-33) liberated from *Plasmodium*-infected Mf may convert these cells into NK-activating Mf through IL-1β/IL-18 receptors [57, 58]. MyD88 in NK cells also participates in this type of NK activation [53, 59].

However, this is not the case in mDC. Although IL-12p70 is produced in mDC in response to the TLR2 ligand BCG-CWS, the role of IL-12 in NK activation is peripheral in the mouse system. There are at least 2 modes of MyD88-dependent NK cell activation in mDC: (1) MyD88 in pDC can couple with TLR7 or TLR9 to activate the IFN-α-inducing pathway, and this pathway also participates in NK cell activation, presumably through type I IFN liberated by pDC [60, 61]; (2) in contrast, MyD88–/– mDC lose the ability to mature in response to TLR2 ligands. For example, the TLR2 ligand Pam2CSK4 facilitates mDC-mediated NK cell activation in the case of wild-type mDC [24]. If wild-type mDC are replaced with MyD88–/– mDC, cell contact-mediated NK activation is hampered even when the cells are stimulated with Pam2 lipopeptide. Although TLR2–/– mDC largely abrogate the NK cell-activating function, slight functional activity remains in TLR2–/– mDC compared with MyD88–/– mDC, suggesting the presence of TLR2-independent MyD88-activating pathways, which may reflect the action of NOD-like receptor inflammatory pathways. Hence, NK cell activation proceeds through TLR2-dependent and TLR2-independent pathways of mDC, both of which involve MyD88. Furthermore, TLR2/MyD88 in NK cells minimally participates in direct NK activation [24, 53].

NK Cell Activation via the TICAM-1 or IPS-1 Pathways in mDC

It has long been established that a dsRNA analog, i.e. polyI:C, serves as an inducer of NK activation [62, 63]. In vivo administration of polyI:C to mice and in vitro exogenous addition of polyI:C to a mixture of BMDC and NK cells both resulted in activation of NK cells. Ex vivo studies using cells from KO mice have helped reveal how polyI:C activates NK cells. PolyI:C, unlike viral or in vitro-transcribed dsRNA, is internalized into the endosome and cytoplasm where it is recognized by TLR3 and MDA5, respectively [9, 11] (fig. 2). IPS-1 is the adaptor for MDA5/RIG-I, while TICAM-1 is the adaptor for TLR3 [32, 43, 64] (fig. 1). Using the gene-disrupted mouse cells of MDA5–/– and TLR3–/– or IPS-1–/– and TICAM-1–/– mDC, the pathway more involved in NK cell activation was examined in vitro [9–11]. In BMDC, the MDA5/IPS-1 pathway is more important than the TLR3/TICAM-1 pathway, as determined by the expression of NK activation marker CD69 and NK cytotoxicity [11], whereas the reverse is true in IFN-γ production by NK cells [64]. NK activation induced in mice injected with polyI:C is completely abrogated in double KO (IPS-1–/– and TICAM-1–/–) mice, suggesting that these 2 pathways are both required for polyI:C-mediated NK activation [10, 11].

Cell contact-mediated NK activation was found to dominantly occur in IRF-3 activation [64] and mDC by depletion studies [65]. Cytokines, including IL-12p40, IL-

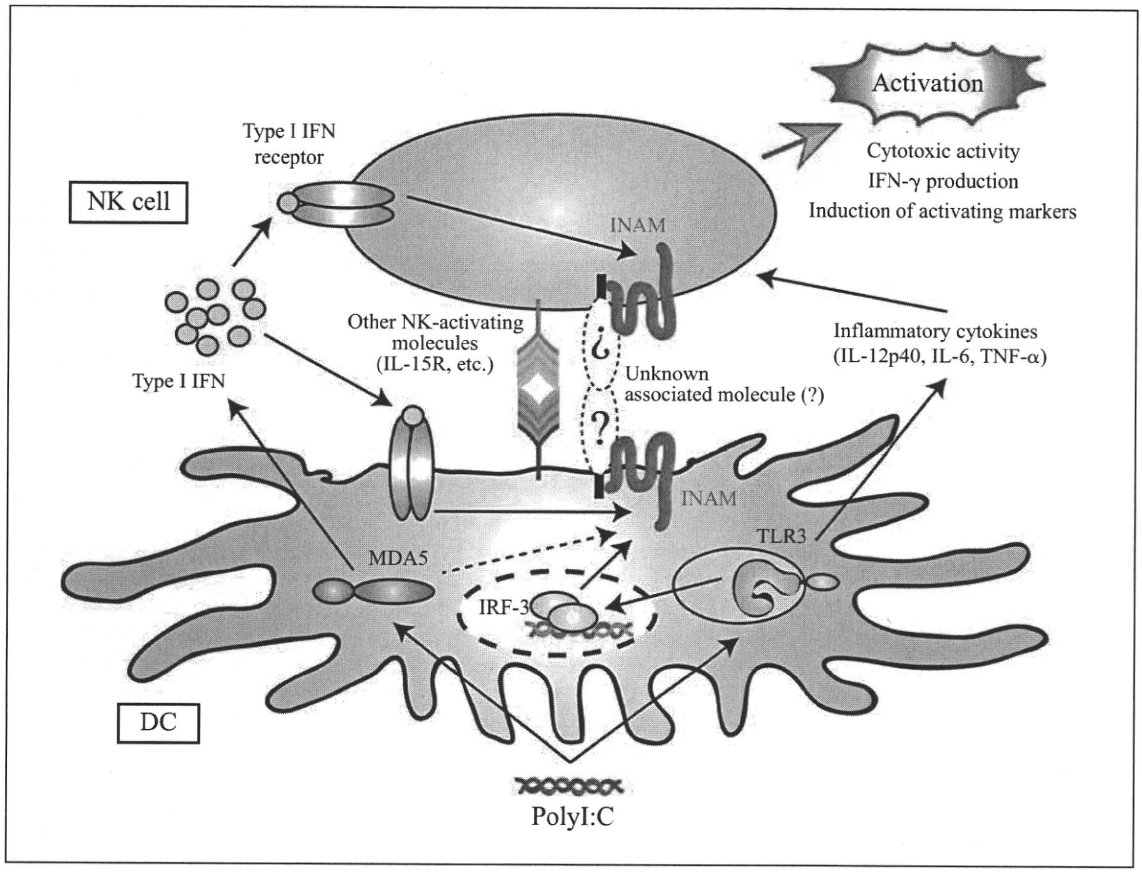

Fig. 2. Induction of INAM-mediated NK cell activation. PolyI:C-stimulated BMDC induce NK cell activation in vitro. INAM is responsible for BMDC contact-mediated NK activation. IRF-3 activation by polyI:C is crucial for INAM upregulation in BMDC, which results in the BMDC-mediated activation of NK cells. Upregulation of INAM on NK cells also facilitates NK cell activation in mDC-NK coculture.

15, and type I IFN, are produced in mDC in response to polyI:C stimulation. Both cell contact and cytokine production mediate NK activation in vitro but cytokines are known to be dispensable for NK activation by polyI:C-stimulated mDC in mice [64]. In vivo injected polyI:C allowed mice to mature splenic DCs [10, 11]. In vivo, bone marrow transplantation chimera analysis suggested that the TLR3-TICAM-1 pathway is important in myeloid cells, along with the IPS-1 pathway in nonmyeloid cells, in driving cytolytic activity by polyI:C [11] (fig. 3). Thus, nonmyeloid-derived soluble factors (mainly IFN-α/β) operate in NK activation in this case. In addition, splenic CD8α+ DC rather than CD8α– DC is crucial for driving NK activation via cell-cell contact [10].

The molecule responsible for mDC-NK contact activation has recently been investigated [64]. There are several polyI:C-inducible membrane-associated molecules in mDC and one of these molecules, designated INAM (IRF-3-dependent NK cell activating molecule), participates in mDC-NK reciprocal activation (fig. 2). However, when overexpressed in non-NK target cells, INAM does not act as an NK-activating ligand; it works only on mDC/Mf for NK activation. Since INAM is predicted to have a tetraspanin-like sequence, unidentified molecules coupling to INAM may foster mDC-NK contact.

NK Cell Activation in Humans and Mice

In human monocyte-derived DC [66] and mouse CD8α+-like human DC (BDCA3+/XCR1+) [67, 68], the early response to dsRNA (including polyI:C and polyA:U) induces the production of IL-12p40 and type I IFN via the TLR3/TICAM-1 pathway. These early-phase cytokines

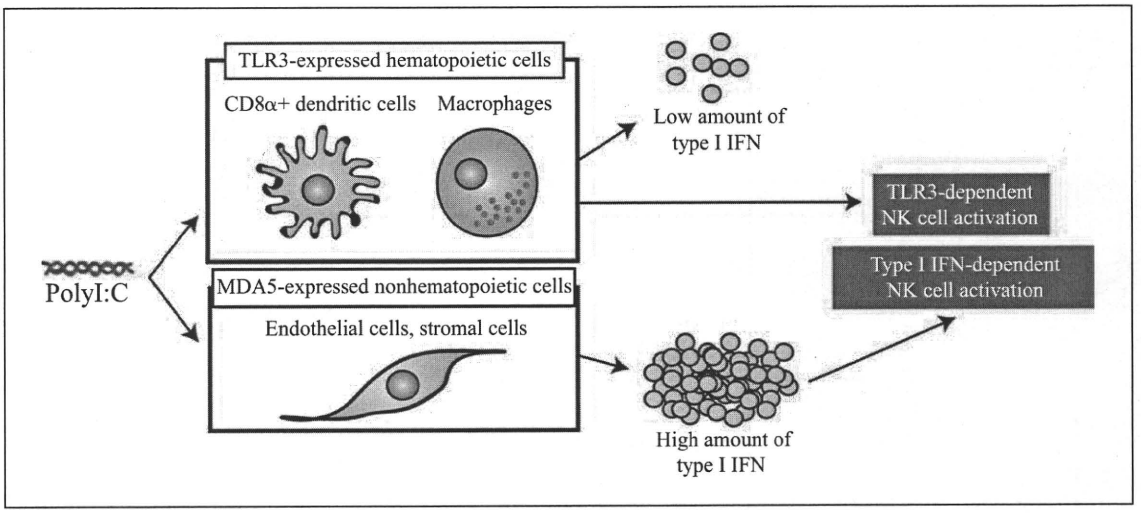

Fig. 3. The IPS-1 pathway in nonmyeloid cells and TLR3 in myeloid cells participate in the activation of NK cells. Mice i.v. injected with polyI:C activate NK cells. Two distinct pathways are involved in NK cell activation in this case: (1) TLR3 in Mf and mDC recognize the i.v. injected polyI:C and drive the internal NK activation pathway, and (2) nonhematopoietic cells recognize the polyI:C by their MDA5 in the cytoplasm to produce a large amount of type I IFN, which in turn activates Mf/DC for NK activation.

play a key role in priming NK cells to induce a low amount of IFN-γ in vitro. In vitro administered dsRNA also activates NK cells via direct stimulation of the RIG-I pathway in NK cells. In the following phase, mDC are recruited to draining lymph nodes to encounter NK cells. Subsequently, mDC-NK contact occurs inducing full maturation of NK cells. At this stage, NK cells engage in significant IFN-γ production. This recent observation is in close agreement with the results reported in human in vitro cocultured liver DC and NK cells [69]. These findings clearly reveal the importance of mDC IL-12p70 and the NK cell RIG-I pathway in NK cell priming in humans.

In mouse in vitro studies, mouse BMDC or CD8α+ splenic DC activate NK cells via cell-cell contact rather than IL-12p70 or type I IFN. BMDC, as well as CD8α+ splenic DC, express TLR3 mRNA, and polyI:C stimulation induces activation of both the TICAM-1 pathway and the IPS-1 pathway [9–11, 64]. IL-12p40 (which is likely the p40 dimer that inhibits IL-12R-derived signaling), instead of IL-12p70, is produced in response to polyI:C in mouse DC-NK coculture studies [64]. A membrane molecule, i.e. INAM, expressed secondary to IRF-3 activation in BMDC or CD8α+ DC stimulates initial DC-mediated NK activation. Full activation of NK cells, including cytolytic activity against target molecules, is provoked only secondarily to DC-NK contact in mice.

In contrast, in vivo studies on NK cell activation have been performed in mice via intravenous (i.v.) injection of polyI:C. NK activation occurs in response to i.v. injected polyI:C, and NK activation has been shown to depend on the MDA5/IPS-1 pathway and TLR3/TICAM-1pathway in KO mice [11] (fig. 3). Surprisingly, in bone marrow chimera studies, initial induction of type I IFN by MDA5 from nonmyeloid cells played a crucial role in splenic DC maturation. CD8α+ DC maturation secondarily triggered NK cell activation. If this is the case, myeloid cell TLR3 and nonmyeloid cell MDA5 actually participate in polyI:C-dependent maturation of splenic DC to drive NK activation, at least at an early phase of i.v. administration in vivo. Presumably, stromal or vascular endothelial cells are a source of MDA5-mediated type I IFN induction, which in turn activates splenic DC. There are several subsets of DC in the mouse spleen. Only CD8α+ DC express high TLR3 and participate in NK activation [10, 70]. On the other hand, intraperitoneal administration of polyI:C first activates Mf in the peritoneal cavity of mice [71]. The route of polyI:C administration may therefore stimulate different RNA sensors to activate IRF-3. IL-12p70 has a minimal role in mouse DC-mediated NK activation.

It is currently unclear which mode of NK activation, TICAM-1 or IPS-1, is dominant in other mammals and vertebrates. NK cells and the TICAM-1 and IPS-1 pathways are conserved across vertebrates. Differential re-

sponses to polyI:C in cytokine production and NK activation in other animals may be partly due to the systemic differences in RNA recognition in different cell types and tissues.

Perspectives

NK cell activation is an important event in the immune response to cancer or infectious diseases. Recent molecular/cellular analyses suggest that the cells and molecular mechanisms involved in NK cell activation differ between in vivo PAMP-stimulated mice and in vitro PAMP-stimulated cell cocultures. A discrepancy also appears in in vitro NK activation studies in humans and mice. The basal IFN-inducing properties have been reported in mice but not in humans [6]. The response to PAMP also differs depending on the delivery routes. Caution is therefore necessary when adapting the results from KO mice to human clinical studies. Only 5 μg of polyI:C sufficiently induces IFN-β from human fibroblasts which express TLR3 on the cell surface, but >150 μg is still insufficient for mouse fibroblasts [72, 73]. Although polyI:C is effective for NK activation, it often induces a life-threatening cytokine storm in mice [74]. A future aim is to activate NK cells with no side effects in human patients. If this can be achieved, NK cell activation could be applied to the establishment of effective vaccines and immunotherapies.

Acknowledgements

We are grateful to Drs. H. Oshiumi, H. Takaki, A. Watanabe, H.H. Aly, S. Yamazaki, and T. Ebihara for invaluable discussions. This work was supported in part by Grants in Aid from the Ministry of Education, Science, and Culture and the Ministry of Health, Labor, and Welfare of Japan, and by the NorthTec Foundation, the Yakult Foundation, the Waxman Foundation, and the Akiyama Life Science Foundation. Financial support from the Sapporo Biocluster 'Bio-S' the Knowledge Cluster Initiative of the MEXT, and the Program of Founding Research Centers for Emerging and Reemerging Infectious Diseases, MEXT, is gratefully acknowledged.

References

1 Trinchieri G: Biology of natural killer cells. Adv Immunol 1989;47:187–376.
2 Bryceson YT, March ME, Ljunggren HG, Long EO: Activation, coactivation, and costimulation of resting human natural killer cells. Immunol Rev 2006;214:73–91.
3 Moretta A: Natural killer cells and dendritic cells: rendezvous in abused tissue. Nat Rev Immunol 2002;2:957–964.
4 Granucci F, Zanoni I, Ricciardi-Castagnoli P: Central role of dendritic cells in the regulation and deregulation of immune responses. Cell Mol Life Sci 2008;65:1683–1697.
5 Joffre O, Nolte MA, Spörri R, Reis e Sousa C: Inflammatory signals in dendritic cell activation and the induction of adaptive immunity. Immunol Rev 2009;227:234–247.
6 Takaoka A, Taniguchi T: New aspects of IFN-α/β signalling in immunity, oncogenesis and bone metabolism. Cancer Sci 2003; 94:405–411.
7 Kono H, Rock KL: How dying cells alert the immune system to danger. Nat Rev Immunol 2008;8:279–289.
8 Seya T, Shime H, Ebihara T, Oshiumi H, Matsumoto M: Pattern recognition receptors of innate immunity and their application to tumor immunotherapy. Cancer Sci 2010;101:313–320.
9 Akazawa T, Ebihara T, Okuno M, Okuda Y, Shingai M, Tsujimura K, Takahashi T, Ikawa M, Okabe M, Inoue N, Okamoto-Tanaka M, Ishizaki H, Miyoshi J, Matsumoto M, Seya T: Antitumor NK activation induced by the Toll-like receptor 3-TICAM-1 (TRIF) pathway in myeloid dendritic cells. Proc Natl Acad Sci USA 2007;104:252–257.
10 Miyake T, Kumagai Y, Kato H, Guo Z, Matsushita K, Satoh T, Kawagoe T, Kumar H, Jang MH, Kawai T, Tani T, Takeuchi O, Akira S: Poly I:C-induced activation of NK cells by CD8 alpha+ dendritic cells via the IPS-1 and TRIF-dependent pathways. J Immunol 2009;183:2522–2528.
11 McCartney S, Vermi W, Gilfillan S, Cella M, Murphy TL, Schreiber RD, Murphy KM, Colonna M: Distinct and complementary functions of MDA5 and TLR3 in poly(I:C)-mediated activation of mouse NK cells. J Exp Med 2009;206:2967–2976.
12 Lanier LL: Up on the tightrope: natural killer cell activation and inhibition. Nat Immunol 2008;9:495–502.
13 Dimasi N, Moretta L, Biassoni R: Structure of the Ly49 family of natural killer (NK) cell receptors and their interaction with MHC class I molecules. Immunol Res 2004;30:95–104.
14 Sun JC, Beilke JN, Lanier LL: Adaptive immune features of natural killer cells. Nature 2009;457:557–561.
15 Cooper MA, Colonna M, Yokoyama WM: Hidden talents of natural killers: NK cells in innate and adaptive immunity. EMBO Rep 2009;10:1103–1110.
16 Newman KC, Riley EM: Whatever turns you on: accessory-cell-dependent activation of NK cells by pathogens. Nat Rev Immunol 2007;7:279–291.
17 Kawai T, Akira S: The roles of TLRs, RLRs and NLRs in pathogen recognition. Int Immunol 2009;21:317–337.
18 Arase H, Mocarski ES, Campbell AE, Hill AB, Lanier LL: Direct recognition of cytomegalovirus by activating and inhibitory NK cell receptors. Science 2002;296:1323–1326.
19 Mandelboim O, Lieberman N, Lev M, Paul L, Arnon TI, Bushkin Y, Strominger JL, Yewdell JW, Porgador A: Recognition of haemagglutinins on virus-infected cells by NKp46 activates lysis by human natural killer cells. Nature 2001;409:1055–1060.
20 Bieback K, Lien E, Klagge IM, Avota E, Schneider-Schaulies J, Duprex WP, Wagner H, Kirschning CJ, ter Meulen V, Schneider-Schaulies S: Hemagglutinin protein of wild-Type measles virus activates Toll-like receptor 2 signaling. J Virol 2002;76:8729–8736.

21 Uehori J, Fukase K, Akazawa T, Uematsu T, Akira S, Funami S, Shingai M, Matsumoto M, Azuma I, Toyoshima K, Kusumoto S, Seya T: Dendritic cell maturation induced by muramyl dipeptide (MDP) derivatives: monoacylated MDP confers TLR2/TLR4 activation. J Immunol 2005;174:7096–7103.
22 Korbel DS, Newman KC, Almeida CR, Davis DM, Riley EM: Heterogenous human NK cell responses to *Plasmodium falciparum*-infected erythrocytes. J Immunol 2005;175:7466–7473.
23 Becker I, Salaiza N, Aguirre M, Delgado J, Carrillo-Carrasco N, Kobeh LG, Ruiz A, Cervantes R, Torres AP, Cabrera N, González A, Maldonado C, Isibasi A: Leishmania lipophosphoglycan (LPG) activates NK cells through Toll-like receptor-2. Mol Biochem Parasitol 2003;130:65–74.
24 Azuma M, Sawahata R, Akao Y, Ebihara T, Yamazaki S, Matsumoto M, Hashimoto M, Fukase K, Fujimoto Y, Seya T: The peptide sequence of diacyl lipopeptides determines dendritic cell TLR2-mediated NK activation. PLoS One 2010;5:e12550.
25 Adachi O, Kawai T, Takeda K, Matsumoto M, Tsutsui H, Sakagami M, Nakanishi K, Akira S: Targeted disruption of the MyD88 gene results in loss of IL-1- and IL-18-mediated function. Immunity 1998;9:143–150.
26 Kawai T, Adachi O, Ogawa T, Takeda K, Akira S: Unresponsiveness of MyD88-deficient mice to endotoxin. Immunity 1999;11:115–122.
27 Honda K, Ohba Y, Yanai H, Negishi H, Mizutani T, Takaoka A, Taya C, Taniguchi T: Spatiotemporal regulation of MyD88-IRF-7 signaling for robust type I interferon induction. Nature 2005;434:1035–1040.
28 Uematsu S, Akira S: Toll-like receptors and type I interferons. J Biol Chem 2007;282:15319–1532.
29 Honda K, Taniguchi T: IRFs: master regulators of signalling by Toll-like receptors and cytosolic pattern-recognition receptors. Nat Rev Immunol 2006;6:644–658.
30 Takaoka A, Yanai H, Kondo S, Duncan G, Negishi H, Mizutani T, Kano S, Honda K, Ohba Y, Mak TW, Taniguchi T: Integral role of IRF-5 in the gene induction programme activated by Toll-like receptors. Nature 2005;434:243–249.
31 Matsumoto M, Funami K, Tanabe M, Oshiumi H, Shingai M, Seto Y, Yamamoto A, Seya T: Subcellular localization of Toll-like receptor 3 in human dendritic cells. J Immunol 2003;171:3154–3162.
32 Oshiumi H, Matsumoto M, Funami K, Akazawa T, Seya T: TICAM-1, an adaptor molecule that participates in Toll-like receptor 3-mediated interferon-beta induction. Nat Immunol 2003;4:161–167.
33 Yamamoto M, Sato S, Hemmi H, Hoshino K, Kaisho T, Sanjo H, Takeuchi O, Sugiyama M, Okabe M, Takeda K, Akira S: Role of adaptor TRIF in the MyD88-independent toll-like receptor signaling pathway. Science 2003;301:640–643.
34 Oshiumi H, Sasai M, Shida K, Fujita T, Matsumoto M, Seya T: TIR-containing adapter molecule (TICAM)-2, a bridging adapter recruiting to toll-like receptor 4 TICAM-1 that induces interferon-beta. J Biol Chem 2003;278:49751–49762.
35 Fitzgerald KA, Rowe DC, Barnes BJ, Caffrey DR, Visintin A, Latz E, Monks B, Pitha PM, Golenbock DT: LPS-TLR4 signaling to IRF-3/7 and NF-kappaB involves the Toll adapters TRAM and TRIF. J Exp Med 2003;198:1043–1055.
36 Fitzgerald KA, McWhirter SM, Faia KL, Rowe DC, Latz E, Golenbock DT, Coyle AJ, Liao SM, Maniatis T: IKK-epsilon and TBK1 are essential components of the IRF3 signaling pathway. Nat Immunol 2003;4:491–496.
37 Sharma S, tenOever BR, Grandvaux N, Zhou GP, Lin R, Hiscott J: Triggering the interferon antiviral response through an IKK-related pathway. Science 2003;300:1148–1151.
38 Sasai M, Oshiumi H, Matsumoto M, Inoue N, Fujita F, Nakanishi M, Seya T: Cutting edge: NF-kappaB-activating kinase-associated protein 1 participates in TLR3/Toll-IL-1 homology domain-containing adapter molecule-1-mediated IFN regulatory factor 3 activation. J Immunol 2005;174:27–30.
39 Ryzhakov G, Randow F: SINTBAD, a novel component of innate antiviral immunity, shares a TBK1-binding domain with NAP1 and TANK. EMBO J 2007;26:3180–3190.
40 Häcker H, Redecke V, Blagoev B, Kratchmarova I, Hsu LC, Wang GG, Kamps MP, Raz E, Wagner H, Häcker G, Mann M, Karin M: Specificity in Toll-like receptor signalling through distinct effector functions of TRAF3 and TRAF6. Nature 2006;439:204–207.
41 Oganesyan G, Saha SK, Guo B, He JQ, Shahangian A, Zarnegar B, Perry A, Cheng G: Critical role of TRAF3 in the Toll-like receptor-dependent and -independent antiviral response. Nature 2006;439:208–211.
42 Yoneyama M, Kikuchi M, Natsukawa T, Shinobu N, Imaizumi T, Miyagishi M, Taira K, Akira S, Fujita T: The RNA helicase RIG-I has an essential function in double-stranded RNA-induced innate antiviral responses. Nat Immunol 2004;5:730–737.
43 Yoneyama M, Kikuchi M, Matsumoto K, Imaizumi T, Miyagishi M, Taira K, Foy E, Loo YM, Gale M Jr, Akira S, Yonehara S, Kato A, Fujita T: Shared and unique functions of the DExD/H-box helicases RIG-I, MDA5, and LGP2 in antiviral innate immunity. J Immunol 2005;175:2851–2858.
44 Saito T, Hirai R, Loo YM, Owen D, Johnson CL, Sinha SC, Akira S, Fujita T, Gale M Jr: Regulation of innate antiviral defenses through a shared repressor domain in RIG-I and LGP2. Proc Natl Acad Sci USA 2007;104:582–587.
45 Li XD, Sun L, Seth RB, Pineda G, Chen ZJ: Hepatitis C virus protease NS3/4A cleaves mitochondrial antiviral signaling protein off the mitochondria to evade innate immunity. Proc Natl Acad Sci USA 2005;102:17717–17722.
46 Loo YM, Owen DM, Li K, Erickson AK, Johnson CL, Fish PM, Carney DS, Wang T, Ishida H, Yoneyama M, Fujita T, Saito T, Lee WM, Hagedorn CH, Lau DT, Weinman SA, Lemon SM, Gale MJ: Viral and therapeutic control of IFN-beta promoter stimulator 1 during hepatitis C virus infection. Proc Natl Acad Sci USA 2006;103:6001–6006.
47 Hornung V, Ellegast J, Kim S, Brzozka K, Jung A, Kato H, Poeck H, Akira S, Conzelmann KK, Schlee M, Endres S, Hartmann G: 5′-Triphosphate RNA is the ligand for RIG-I. Science 2006;314:994–997.
48 Pichlmair A, Schulz O, Tan CP, Naslund TI, Liljestrom P, Weber F, Reis e Sousa C: RIG-I-mediated antiviral responses to single-stranded RNA bearing 5′-phosphates. Science 2006;314:997–1001.
49 Kato H, Takeuchi O, Sato S, Yoneyama M, Yamamoto M, Matsui K, Uematsu S, Jung A, Kawai T, Ishii KJ, Yamaguchi O, Otsu K, Tsujimura T, Koh CS, Reis e Sousa C, Matsuura Y, Fujita T, Akira S: Differential roles of MDA5 and RIG-I helicases in the recognition of RNA viruses. Nature 2006;441:101–105.
50 Kato H, Sato S, Yoneyama M, Yamamoto M, Uematsu S, Matsui K, Tsujimura T, Takeda K, Fujita T, Takeuchi O, Akira S: Cell type-specific involvement of RIG-I in antiviral response. Immunity 2005;23:19–28.
51 Kochs G, Bauer S, Vogt C, Frenz T, Tschopp J, Kalinke U, Waibler Z: Thogoto virus infection induces sustained type I interferon responses that depend on RIG-I-like helicase signaling of conventional dendritic cells. J Virol 2010;84:12344–12350.
52 Matsumoto M, Oshiumi H, Seya T: Antiviral responses induced by the TLR3 pathway. Rev Med Virol 2011, Epub ahead of print.
53 Martinez J, Huang X, Yang Y: Direct TLR2 signaling is critical for NK cell activation and function in response to vaccinia viral infection. PLoS Pathog 2010;6:e1000811.
54 Sawaki J, Tsutsui H, Hayashi N, Yasuda K, Akira S, Tanizawa T, Nakanishi K: Type 1 cytokine/chemokine production by mouse NK cells following activation of their TLR/MyD88-mediated pathways. Int Immunol 2007;19:311–320.
55 Hamerman JA, Ogasawara K, Lanier LL: Cutting edge: Toll-like receptor signaling in macrophages induces ligands for the NKG2D receptor. J Immunol 2004;17:2001–2005.

56 Cole LE, Santiago A, Barry E, Kang TJ, Shirey KA, Roberts ZJ, Elkins KL, Cross AS, Vogel SN: Macrophage proinflammatory response to *Francisella tularensis* live vaccine strain requires coordination of multiple signaling pathways. J Immunol 2008;180:6885–6891.
57 Adachi K, Tsutsui H, Kashiwamura S, Seki E, Nakano H, Takeuchi O, Takeda K, Okumura K, Van Kaer L, Okamura H, Akira S, Nakanishi K: *Plasmodium berghei* infection in mice induces liver injury by an IL-12- and Toll-like receptor/myeloid differentiation factor 88-dependent mechanism. J Immunol 2001;167:5928–5934.
58 Baratin M, Roetynck S, Lépolard C, Falk C, Sawadogo S, Uematsu S, Akira S, Ryffel B, Tiraby JG, Alexopoulou L, Kirschning CJ, Gysin J, Vivier E, Ugolini S: Natural killer cell and macrophage cooperation in MyD88-dependent innate responses to *Plasmodium falciparum*. Proc Natl Acad Sci USA 2005; 102:14747–14752.
59 Akao Y, Ebihara T, Masuda H, Saeki Y, Akazawa T, Hazeki K, Hazeki O, Matsumoto M, Seya T: Enhancement of antitumor natural killer cell activation by orally administered Spirulina extract in mice. Cancer Sci 2009; 100:1494–501.
60 Krug A, French AR, Barchet W, Fischer JA, Dzionek A, Pingel JT, Orihuela MM, Akira S, Yokoyama WM, Colonna M: TLR9-dependent recognition of MCMV by IPC and DC generates coordinated cytokine responses that activate antiviral NK cell function. Immunity 2004;21:107–119.
61 Hoshino K, Sugiyama T, Matsumoto M, Tanaka T, Saito M, Hemmi H, Ohara O, Akira S, Kaisho T: IkappaB kinase-alpha is critical for interferon-alpha production induced by Toll-like receptors 7 and 9. Nature 2006; 440:949–953.
62 Djeu JY, Heinbaugh JA, Holden HT, Herberman RB: Augmentation of mouse natural killer cell activity by interferon and interferon inducers. J Immunol 1979;122: 175–181.
63 Wiltrout RH, Salup RR, Twilley TA, Talmadge JE: Immunomodulation of natural killer activity by polyribonucleotides. J Biol Response Mod 1985;4:512–517.
64 Ebihara T, Azuma M, Oshiumi H, Kasamatsu J, Iwabuchi K, Matsumoto K, Saito T, Taniguchi T, Matsumoto M, Seya T: Identification of a polyI:C-inducible membrane protein that participates in dendritic cell-mediated natural killer cell activation. J Exp Med 2010;207:2675–2687.
65 Lucas M, Schachterle W, Oberle K, Aichele P, Diefenbach A: Dendritic cells prime natural killer cells by trans-presenting interleukin 15. Immunity 2007;26:503–517.
66 Matsumoto M, Funami K, Tanabe M, Oshiumi H, Shingai M, Seto Y, Yamamoto A, Seya T: Subcellular localization of Toll-like receptor 3 in human dendritic cells. J Immunol 2003;171:3154–3162.
67 Crozat K, Guiton R, Contreras V, Feuillet V, Dutertre CA, Ventre E, Vu Manh TP, Baranek T, Storset AK, Marvel J, Boudinot P, Hosmalin A, Schwartz-Cornil I, Dalod M: The XC chemokine receptor 1 is a conserved selective marker of mammalian cells homologous to mouse CD8alpha+ dendritic cells. J Exp Med 2010;207:1283–1292.
68 Bachem A, Güttler S, Hartung E, Ebstein F, Schaefer M, Tannert A, Salama A, Movassaghi K, Opitz C, Mages HW, Henn V, Kloetzel PM, Gurka S, Kroczek RA: Superior antigen cross-presentation and XCR1 expression define human CD11c+CD141+ cells as homologues of mouse CD8+ dendritic cells. J Exp Med 2010;207:1273–1281.
69 Tu Z, Bozorgzadeh A, Pierce RH, Kurtis J, Crispe IN, Orloff MS: TLR-dependent cross talk between human Kupffer cells and NK cells. J Exp Med 2008;205:233–244.
70 Jelinek I, Leonard JN, Price GE, Brown KN, Meyer-Manlapat A, Goldsmith PK, Wang Y, Venzon D, Epstein SL, Segal DM: TLR3-specific double-stranded RNA oligonucleotide adjuvants induce dendritic cell cross-presentation, CTL responses, and antiviral protection. J Immunol 2011;186:2422–2429.
71 Wu CY, Monie A, Yang HY, Wu Tc, Hung CF: Intraperitoneal administration of polyI:C with polyethylenimine leads to significant antitumor immunity against murine ovarian tumors. Cancer Immunol Immunother 2011, in press.
72 Matsumoto M, Kikkawa S, Kohase M, Miyake K, Seya T: Establishment of a monoclonal antibody against human Toll-like receptor 3 that blocks double-stranded RNA-mediated signaling. Biochem Biophys Res Commun 2002;293:1364–1369.
73 Matsumoto M, Seya T: TLR3: interferon induction by double-stranded RNA including poly(I:C). Adv Drug Deliv Rev 2008;60:805–812.
74 Absher M, Stinebring WR: Toxic properties of a synthetic double-stranded RNA: endotoxin-like properties of poly I – poly C, an interferon stimulator. Nature 1969;223:715–717.

[Prion 2:2, 73-80; April/May/June 2008]; ©2008 Landes Bioscience

Research Paper

Anti-bovine prion protein RNA aptamer containing tandem GGA repeat interacts both with recombinant bovine prion protein and its β isoform with high affinity

Kazuyoshi Murakami,[1,2] Fumiko Nishikawa,[2] Ken Noda,[3] Takashi Yokoyama[4] and Satoshi Nishikawa[1,2,*]

[1]Graduate School of Life and Environmental Science; University of Tsukuba; Tennodai; Tsukuba, Ibaraki Japan; [2]Age Dimension Research Center; National Institute of Advanced Industrial Science and Technology (AIST); Tsukuba, Ibaraki Japan; [3]National Veterinary Assay Laboratory (NVAL); Ministry of Agriculture; Forestry and Fisheries; Kokubunji, Tokyo Japan; [4]Prion Disease Research Center; National Institute of Animal Health (NIAH); Tsukuba, Ibaraki Japan

Abbreviations: bPrP, bovine prion protein; bPrP-β, β isoform of bovine prion protein; bPrP (102–241), amino acids 102–241 of bovine prion protein; bPrP (132–241), amino acids 132–241 of bovine prion protein; mPrP, mouse prion protein; PrP^{C}, cellular isoform of prion protein; PrP^{Sc}, scrapie isoform of prion protein; SELEX, systematic evolution of ligands by exponential enrichment; CD, circular dichroism

Key words: RNA aptamer, prion protein, SELEX, GGA repeat, G-quadruplex

In order to obtain RNA aptamers against bovine prion protein (bPrP), we carried out in vitro selection from RNA pools containing a 55-nucleotide randomized region to target recombinant bPrP. Most of obtained aptamers contained conserved GGA tandem repeats $(GGA)_4$ and aptamer #1 (apt #1) showed a high affinity for both bPrP and its β isoform (bPrP-β). The sequence of apt #1 suggested that it would have a G-quadruplex structure, which was confirmed using CD spectra in titration with KCl. A mutagenic study of this conserved region, and competitive assays, showed that the conserved $(GGA)_4$ sequence is important for specific binding to bPrP and bPrP-β. Following 5'-biotinylation, aptamer #1 specifically detected PrP^{c} in bovine brain homogenate in a Northwestern blotting assay. Protein deletion mutant analysis showed that the bPrP aptamer binds within 25–131 of the bPrP sequence. Interestingly, the minimized aptamer #1 (17 nt) showed greater binding to bPrP and bPrP-β as compared to apt #1. This minimized form of aptamer #1 may therefore be useful in the detection of bPrP, diagnosis of prion disease, enrichment of bPr and ultimately in gaining a better understanding of prion diseases.

Introduction

The prion protein (PrP) has two alternative forms: a normal cellular protein (PrP^{C}), which is a soluble α-helix rich isoform, and an insoluble β-sheet rich abnormal isoform[1] known as the protease-resistant form (PrP^{Sc}).[2] The detailed mechanism of the structural conversion between the soluble and insoluble forms remains unknown. PrP^{C} is almost ubiquitously expressed and highly conserved in mammals, being anchored on the surface of cells. To gain a better insight into its putative role, much research has gone towards the discovery of molecules that bind prion protein. Of those identified, the most notable are divalent metal ions, several proteins and nucleic acids.[3] Knowledge of the function of PrP would contribute towards a better understanding of the processes involved in both the amplification of the infectious agent and the neuronal damage leading to the neuro-degeneration observed in prion diseases. As concerns about the transmission of prion disease in the fields of medicine and food safety increase, there is an increasing demand for an understanding of the processes by which PrP^{Sc} can be detected and addressed.[4,5]

Specific anti-PrP probes, which have high specificity and sensitivity, are required for the diagnosis of prion diseases. Clarification of the binding mechanism between PrP and such probes will assist structural study of PrP. Aptamers are artificial nucleotides derived from systematic evolution of ligands by exponential enrichment (SELEX),[6,7] which bind a wide range of targets with a high affinity and specificity, as is seen with antibodies.[8,9] Using this method, many aptamers specific to PrP^{10-20} and PrP^{Sc},[12,13] have been isolated.

Recently we have performed an in vitro selection for mouse PrP using an RNA pool with a 30 nt randomized region.[16] To prepare a repertoire of anti-PrP RNA aptamers, we carried out SELEX for recombinant bPrP and analyzed for bPrP and bPrP-β. The obtained major RNA aptamers bind to both bPrP and bPrP-β. They possessed tandem GGA repeats $(GGA)_4$ as a consensus sequence, and suggested to form a parallel G-quadruplex structure in the presence of K^{+} ions. We identified that this core sequence is important for specific binding to bovine PrPs and increased the affinity and selectivity by redesigning this core sequence.

Results

In vitro selection. To obtain RNA aptamers targeting recombinant bPrP, we carried out SELEX using 97-nt RNA pool that has

*Correspondence to: Satoshi Nishikawa; Age Dimension Research Center; National Institute of Advanced Industrial Science and Technology (AIST); Tsukuba, Ibaraki 305-8566 Japan; Tel.: +81.29.861.6097; Fax: +81.29.861.6095; Email: satoshi-nishikawa@aist.go.jp

Submitted: 08/25/08; Accepted: 09/17/08

Previously published online as a *Prion* E-publication:
http://www.landesbioscience.com/journals/prion/article/7024

55-nt randomized sequences. To increase the selection stringency, we applied the following selection pressures (Table 1): (1) decreased protein concentration and reaction time, and increased washing volumes; (2) increased tRNA concentration as a non-specific competitor; and (3) increased concentration of anti-mPrP RNA aptamer[16] as a specific competitor. Furthermore we carried out mutagenic PCR[21] to introduce mutations into concentrated sequences (see Materials and Methods). As the enrichment of specific binding RNAs for bPrP was observed in the iterative process (data not shown), G10 RNA pool for bPrP was cloned and sequenced. Interestingly, all RNAs contained tandem GGA repeats, mainly four continuous GGA triplet repeats $(GGA)_4$ (shown underlined in Table 2).

Binding affinities of apt #1 against bPrP or bPrP-β. The representative RNA aptamers designated apt #1 and apt #6 were analyzed. To determine their respective K_d values, a filter binding assay was performed using 10 nM RNA and various concentrations of bPrP or bPrP-β in selection buffer [20 mM Tris-HCl (pH 7.5), 100 mM NaCl]. Apt #1 showed a higher affinity (Fig. 1, K_d = 82 ± 21 nM for bPrP) than that of apt #6 (data not shown, K_d = 166 ± 55 nM for bPrP). Because of the structural difference between bPrP and bPrP-β, binding affinity of both RNA aptamers for bPrP-β are over 10-fold lower than those for bPrP. As it demonstrated a higher affinity than apt #6, we focused on apt #1 in subsequent analyses.

The $(GGA)_4$ sequence suggested that it forms a G-quartet structure. The formation of a G-quartet structure is stabilized by monovalent cations such as K^+ and Na^+ ions.[25,26] In general, DNA/RNA G-quadruplexes bind K^+ over Na^+ ions.[25,26] As is clearly shown in Figure 1, binding affinities for both proteins bPrP and bPrP-β in 10 mM K^+ ion (K_d = 31 nM and 220 nM, respectively; solid lines) were increased in comparison with 100 mM Na^+ ion (dashed lines). We also tested apt #1 binding without salt (K_d = 50 nM for bPrP and ≥1000 nM for bPrP-β; data not shown). The presence of potassium ions conferred a greater affinity of apt #1 to bPrPs, which was particularly profound for bPrP-β. We therefore prepared a buffer solution containing K^+ ions to be used in subsequent analyses on apt #1 (20 mM Tris-HCl (pH 7.5), 10 mM KCl).

Detection of $bPrP^C$ in bovine brain homogenate using apt #1. To test the ability of apt #1 to detect $bPrP^C$, we performed Northwestern blotting using a 5'-biotinylated apt #1 (Bi#1) with streptavidin-alkaline phosphatase conjugates (SA-AP) as a secondary probe (left in Fig. 2A). Bi#1 detected the three types of $bPrP^C$ (non-, mono- and di-glycosylated forms of PrP^C; lane 1) in bovine brain homogenate as well as antibody T2 (lane 2). The epitope of antibody T2 is located between amino acids 147 and 152.[23] This result indicates that apt #1 is applicable as a detection tool for bPrP and may perform as well as antibodies.

Table 1 **In vitro selection conditions for recombinant bPrP**

Round of selection	RNA (μM)	bPrP (μM)	tRNA (μM)	Anti-PrP RNA aptamer[16] (μM)	Time (min)
1	10	2	0	0	60
2	6	0.4	10	0	30
3	4	0.2	40	8	20
4	3	0.1	100	16	15
5	2	0.3	100	32	10
6	2	0.05	100	48	10
7	2	0.05	*6	0	10
8**	2	0.05	100	64	10
9**	2	0.05	100	64	10
10	6	0.05	100	96	10

*U_{13} was used instead of tRNA. **The mutagenic PCR was introduced.

The detection limit of bPrP with Bi#1 was approximately 30 ng (spot 6 in the upper of Fig. 2B) using dot blot analysis in the presence of poly (U) as a non-competitive binder. A negative control BiC#1 that has the complementary sequence of apt #1, showed a detection limit 240 ng (spot 3 in the lower of Fig. 2B), indicating specific binding of apt #1 against $bPrP^C$.

Conserved region $(GGA)_4$ suggests a parallel G-quadruplex. To examine the structure of apt #1, we measured CD spectra of the aptamer in the different concentrations of K^+ ion. It is known that a parallel G-quadruplex gives a positive CD peak at 260 nm, while an antiparallel G-quadruplex gives a positive CD peak at 295 nm either with or without a positive CD peak at 260 nm in the presence of monovalent cations.[27,28] A peak was observed at 260 nm of CD and the peak intensity increased as the concentration of K^+ ions increased, with maximum peak intensity at 10 mM KCl (Fig. 3A). This result suggests that apt #1 forms a parallel G-quadruplex in the presence of K^+ ion, with saturation occurring at 10 mM KCl. We also confirmed no increase of peak intensity at 260 nm in the presence of K^+ ion on the apt #1 mutant with substitutions of G tracts in the conserved $(GGA)_4$ region (data not shown).

Matsugami et al. reported that $d(GGA)_4$ folds into an intramolecular G-quadruplex composed of a G:G:G:G tetrad and a G(:A):G(:A):G(:A):G heptad with parallel orientation under physiological K^+ conditions[24] (Fig. 3B). The CD spectra of apt #1 (Fig. 3A) showed a similar pattern with that of $d(GGA)_4$. Although direct evidence is lacking, we believe that apt #1 also forms the similar type of the parallel G-quadruplex structure. Previous reports

Table 2 **Sequences of randomized regions and majorities of isolated RNA aptamers against recombinant bPrP**

Name of clone	Number of clones	Sequence of randomized region
#1	14/30	5'-CAAUCCAUUCAUCUCUCGAAUGAGGAAGUAGCCCAAGAGGAGGAGGAGGAUGAGC-3'
#6	11/30	5'-ACCUUCUGUUCAUAUCGUGACCAACCCAAUAGAUUGUGAUAAAGGAGGAGGAGGA-3'
#20	3/30	5'-UUGCCAAUAGCCCUACGGAGGAGGAGGCUGGACUAUAGACAGUUUACUUAAUAAA-3'
others		5'-CGCUCUGCCUGCGACCCAUCGACGUGAGUUUGCGAAAAAAGGAGGAGGAGGA-3'
		5'-UAGCCCCCCUAGGAGCCGCUUGUGAUAAGAGUUCAAAUUGGAGGAGGUGGAUUGA-3'

The conserved GGA triplet repeats $(GGA)_4$ are underlined involving its one point mutations.

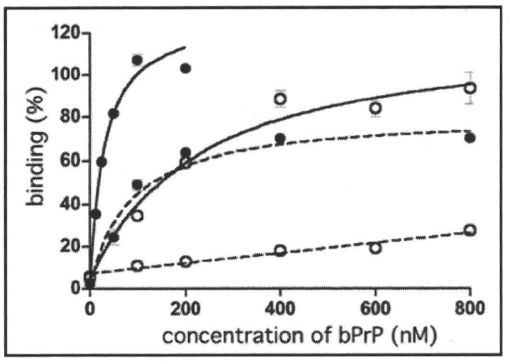

Figure 1. Binding of apt #1 to bPrP and bPrP-β. Binding curves of apt #1 to bPrP and bPrP-β are shown by closed circles and open circles, respectively. Solid and dashed lines represent different buffer conditions: 10 mM K^+ and 100 mM Na^+, respectively. The binding data are analyzed by GraphPad PRISM (see Materials and Methods).

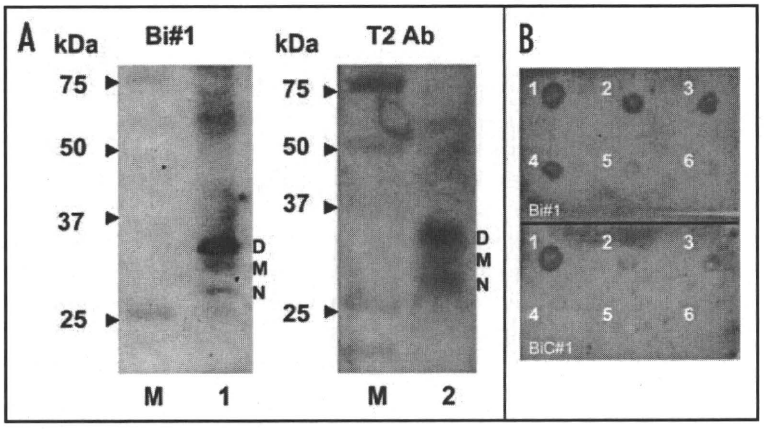

Figure 2. Detection of $bPrP^C$ in bovine brain homogenate and dot-blotting assay using a biotinylated apt #1 (Bi#1). (A) Bovine brain homogenate was analyzed using SDS-PAGE and subsequently with Northwestern blotting. $bPrP^C$ (lane 1 and 2) was detected using Bi#1 (left) and T2 antibody (right). Lane M represents protein molecular weight markers. N, M and D indicate non-, mono- and di-glycosilated PrP isoforms, respectively. (B) Dot-blotting assay of recombinant bPrP using Bi#1 or BiC#1. Number 1 represents cross-linked 5'-biotinylated RNA (Bi#1, BiC#1). Numbers 2–6 represent decreasing concentration of mounted bPrP (ng) as follows: 2 = 480, 3 = 240, 4 = 120, 5 = 60, 6 = 30.

have described G-quadruplex forming RNA aptamers for PrP,[10,11] but sequences are different from described here.

Aptamer binding sites locate amino acids 25–131. To investigate the apt #1 binding region of bPrP, we performed binding analysis with deleted proteins: bPrP (102–241) and bPrP (132–241) (Fig. 4A). Apt #1 bound strongly to full length bPrP (K_d = 31 nM), while K_d value of the deletion variant bPrP (102–241) (≥1000 nM; indicated with triangles) increased more than 30-fold compared with bPrP. Apt #1 could not bind to variant bPrP (132–241). Consequently, the binding region for apt #1 is located within amino acid residues 25–131, underlined in Figure 4B. Deletion of N-terminal 25–101 residues produced a strong effect for the aptamer binding. This suggests that this region is the main binding site as well as an anti-mPrP aptamer.[16] Mercey et al. reported that the two lysine clusters (amino acids 25–32 and 102–110 in ovine PrP) are primary nucleic acids binding sites, the former region showing stronger binding than the latter.[15] Considering these results, it seems that apt #1 is also likely to bind to the two lysine clusters, although there is no homology between apt #1 and ovine-PrP aptamers.

The conserved region $(GGA)_4$ is important for binding to bPrP or bPrP-β. To investigate the correlation between binding affinity and G-quadruplex structure of the conserved $(GGA)_4$, we prepared several mutants of the $(GGA)_4$ region (m1–m5) and analyzed their affinities compared to bPrP and bPrP-β. The K_d values for different mutants are shown in Table 3. All #1 mutants showed decrease of binding ability to bPrP-β. The conserved $(GGA)_4$ is therefore important for binding to bPrP-β. In the case of interactions with bPrP, all mutants except m4 showed moderate decrease in binding affinity (1.8–2.5-fold). This is due to the ability of PrP to bind to nucleic acids.[29,30]

Since we could not verify the specific binding of mutants to bPrP from the determined K_d values, we carried out competitive binding analysis using the labeled apt #1 in the presence of elevated amounts of unlabeled competitors (Fig. 5). We used non G-quadruplex forming competitor (m5) and probable G-quadruplex forming competitors (m7, m8, apt #1). It was demonstrated that apt #1 was the best competitor, and all probable G-quadruplex forming competitors competed with apt #1 for binding to bPrP in dose-dependent manner. There are small differences of displacement efficiency among apt #1, m7 and m8. By comparing the competing ability of G-quadruplex forming RNAs m7, m8 and apt #1, the adenine residues in $(GGA)_4$ are also important for binding to bPrP. Non G-quadruplex forming competitor (m5) showed weak competition in the presence of K^+ ion. Under the no salt condition m5 competed with apt #1 in the similar level of apt #1 (Fig. 5B). This means that binding ability of apt #1 to bPrP is specific binding in the presence of K^+ ion.

Minimization of apt #1 retained the binding ability to bPrP and bPrP-β. Since the conserved region $(GGA)_4$ of apt #1 plays important role for specific binding to bPrP and bPrP-β, we minimized the aptamer to a 12-nt RNA $r(GGA)_4$ and measured K_d values (Table 4). Compared with apt #1, $r(GGA)_4$ showed better affinity for bPrP (K_d = 8.5 nM) and similar K_d value for bPrP-β (K_d = 280 nM). We then examined $d(GGA)_4$, which forms the unique G-quadruplex structure shown in Figure 3B.[24] This revealed that $d(GGA)_4$ showed a strikingly lower affinity for both bPrP and bPrP-β, compared to $r(GGA)_4$. This result suggests that $r(GGA)_4$ has a different G-quadruplex structure with that of $d(GGA)_4$.

To test the RNA sequence specificity of $r(GGA)_4$, we analyzed the binding of R14, which contains GGA residues and forms another type of intramolecular G-quadruplex consisting of tetrad and hexad in the presence of K^+.[31] As shown in Table 4, R14 showed greater affinity for both proteins compared to $d(GGA)_4$, but lower affinity than $r(GGA)_4$. Hence the conserved tandem GGA repeat $(GGA)_4$ is the important region for binding to bPrP and bPrP-β, and the minimized 12-nt RNA retained this binding ability.

Adenine stretch attached at 5'-site of $(GGA)_4$ enhanced the binding affinity for bPrP-β. Besides of conserved region $(GGA)_4$, adenine tracts (3–6 residues) were frequently observed at the 5'-site of $(GGA)_4$ in obtained RNA aptamers (Table 2). The capacity of these adenine sequences to bind to bPrPs was investigated. The

sequence of constructs and their K_d values are shown in Table 5. Binding affinities were almost the same (K_d = 9–17 nM) for full-length bPrP. For truncated variant bPrP (102–241), they also showed the same level of binding affinities (K_d = 160–270 nM) except r(GGA)$_4$-19 attached 7 adenines (K_d = 540 nM). However with regard to bPrP-β, the five adenine stretch r(GGA)$_4$-17 showed the lowest K_d value (K_d = 78 nM), followed by the four adenines stretch r(GGA)$_4$-16 (K_d = 92 nM). The optimal numbers of adenine correspond with the trend observed in the RNA aptamers.

As reported previously, amino acids 23–90 (human numbering) of PrP interact with nucleic acids in a specific or non-specific manner.[32] Short RNAs including r(GGA)$_4$-17 bound to bPrP (102–241) (probably amino acids residues 102–131 from the binding result of #1 in Fig. 4) in a specific manner. Therefore, like an antibody, r(GGA)$_4$-17 shown in Table 5 may recognize PrP27-30, which is a proteinase K (PK) resistant fragment following removal of the N-terminal region (approximately up to amino acid position 90 in mPrP).[33-36]

Discussion

In this study, we described an in vitro selection of RNA aptamers against recombinant bPrP. All selected RNA aptamers contained the four repeats of a two guanine containing sequence and most of RNAs contained the conserved sequence (GGA)$_4$ (Table 2). Our findings suggest that apt #1 can be used to detect PrP^C in bovine brain homogenate, a process which more conventionally employs an antibody with an immuno-blotting assay (Fig. 2). By collecting CD spectra in increasing concentrations of KCl, apt #1 probably forms a parallel G-quadruplex derived from the (GGA)$_4$ sequence.

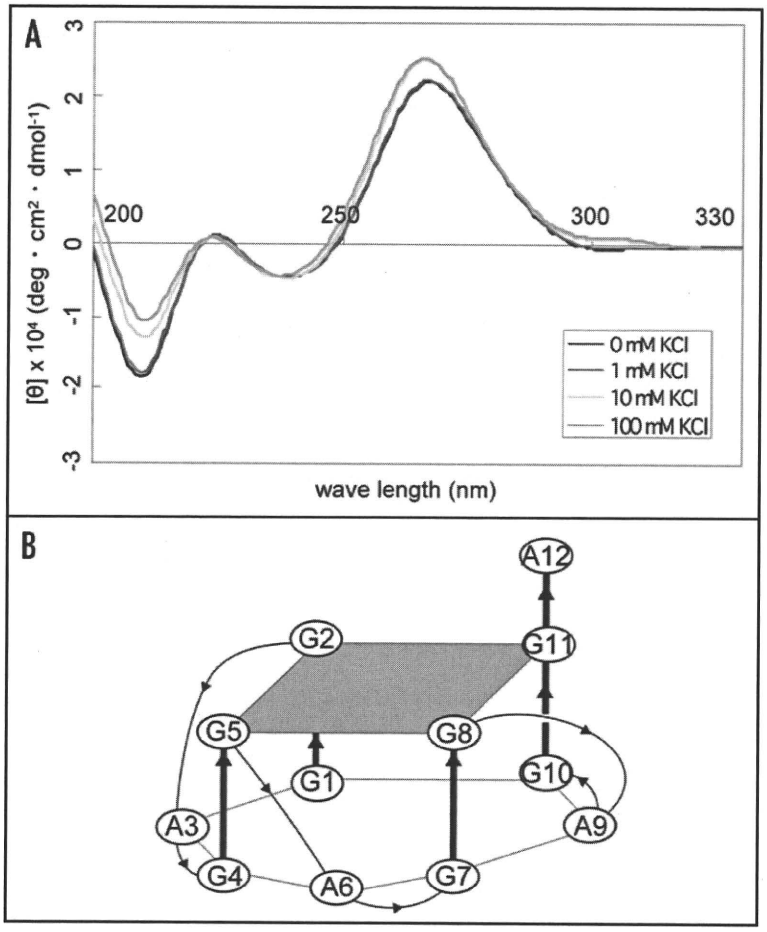

Figure 3. CD spectra of apt #1 and r(GGA)$_4$-15 in the presence of KCl. CD spectra were measured at 20°C in titration with KCl (0, 1, 10, 100 mM). (A) CD spectra of 10 μM apt #1. (B) The structure of d(GGA)$_4$.[24]

It has been reported that the proposed G-quadruplex structure plays a critical role in the binding to PrP.[10,11] Among the reported anti-PrP RNA aptamers containing GGA repeats, anti-syrian golden hamster PrP aptamers contain GGGA repeat interacting with amino acids 23–52,[10] and aptamer DP7 targeted to amino acids 90–129 of human PrP involves GGA repeats.[11] Anti-mPrP aptamer 60–3 used as a competitor in this study also contains GGAGG repeat interacting with amino acids 23–119.[16] The aptamer 60–3 binds to bPrP in the presence of Na^+,[16] however it did not show enhanced bindings to both bPrP and bPrP-β in the presence of K^+ (data not shown). The conserved sequence of tandem GGA repeat (GGA)$_4$ is isolated only in this study. Considering the high frequent appearance of GGA observed in anti-PrP RNA aptamers, GGA repeat must be meaningful for specific binding to PrPs.

We confirmed that the conserved sequence (GGA)$_4$ is important for specific binding to both bPrP and bPrP-β by investigating the effect of substitutions in this region (Table 3) and competitive binding analysis (Fig. 5). Amongst G-quartets which form small DNA and RNAs involving a GGA repeat, r(GGA)$_4$ showed the best affinity to both bPrP and bPrP-β indicating the minimal sequence required for the sequence specificity for preferential binding (Table 4). d(GGA)$_4$ and R14,[31] form similar intramolecular parallel G-quadruplexes consisting of tetrad-heptad and tetrad-hexad, respectively.[24] R14 showed better binding to bPrP and bPrP-β compared to d(GGA)$_4$. This preferential binding may be derived either from the RNA molecule or differences in the tertiary G-quadruplex structures. To clarify the relationships between binding and structure, we are in the process of investigating these structures in more detail.

The binding affinity of bPrP-β with the G_0 RNA pool was notably low (data not shown). The recombinant amyloidogenic prion protein, bPrP-β, is generated through chemical treatment of recombinant bPrP which enhances the formation of the β-sheet secondary structure in the C-terminal region.[37] The N-terminus of PrP (amino acids 23–120 in mPrP) is a flexible non-structural region and the C-terminus of PrP is preserved in the globular three-dimensional structure.[38] It is known that the N-terminal region of PrP interacts with nucleic acids in non-specific and/or specific manner.[29,30,32] In an NMR study of the interaction between murine recombinant PrP and RNA aptamer SAF93,[12,43-59] it was observed that part of the N-terminal domain is modified after interaction with RNA.[39] From these experimental results, it can be deduced that the environment of N-terminal regions also differ between bPrP and bPrP-β. One possibility is that the packed structure of the C-terminal region, which contains higher numbers of β-sheets in bPrP-β, causes a narrowing of free space and a decrease in structural flexibility in the N-terminal region, resulting in poor acceptability of nucleic acids and induced fitting. Finally, we showed that the binding ability for

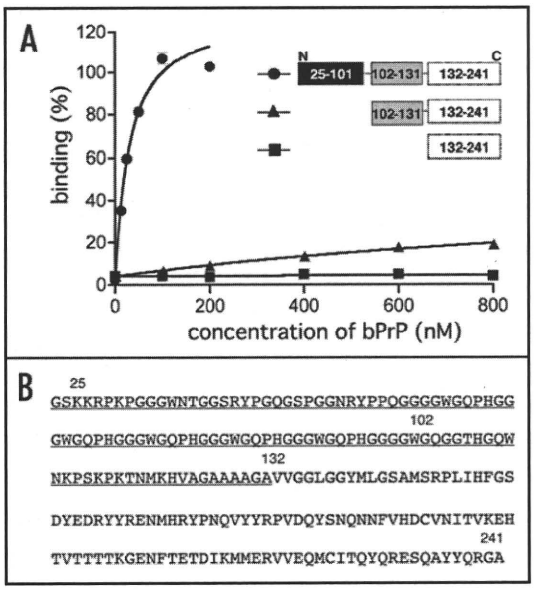

Figure 4. Binding affinity of anti-bPrP aptamer apt #1 for deletion variants of bPrP. (A) Circles, triangles and squares indicate full length bPrP (25–241), bPrP (102–241) and bPrP (132–241), respectively. (B) The amino-acid sequence alignment of bPrP. The apt #1 binding region is underlined.

Table 3 Sequences and binding affinities of different mutants

aptamers	sequence	K_d (nM)	
		bPrP	bPrP-β
apt #1	5'-GGAGGAGGAGGA-3'	31 ± 6	220 ± 67
m1	5'-GGAGGAGGA-3'	79 ± 24	≥1000
m2	5'-GGAGGA-3'	75 ± 28	≥1000
m3	5'-(no GGA repeat)-3'	55 ± 24	≥1000
m4	5'-UUUUUUUUUUUU-3'	134 ± 42	≥1000
m5	5'-UUAUUAUUAUUA-3'	56 ± 16	≥1000

bPrP-β could be improved by minimization of apt #1 to a 17 nt RNA containing an adenosine sequence at the 5'-site of $(GGA)_4$.

By investigating the binding properties of deletion variants of bPrP, we identified the N-terminal region of bPrP, amino acids 25–131, as being a key region for apt #1 binding. Apt #1 could bind to amino acids 102–131 of bPrP. It is known that amino acids 25–101 (23–90 in hPrP) contain the nucleic acid binding site.[32] Notably, the additional N-terminal binding region 102–131 provides apt #1 with specific binding activity. Furthermore, it conferred the ability of the minimized aptamer to bind with both bPrP and bPrP-β with high affinity.

Aptamers, with their high ligand specificity, can enrich a target molecule from biological samples. For example, RNA ligands have been successfully used for the concentration of PrP^C and PK-resistant PrP taken from serum, urine[32] and brain homogenate.[40] Previously, we also used anti-mPrP aptamer for bead-based purification and concentration of PrP^C from mouse brain homogenate.[16] Takemura et al. proposed that PrP^{Sc}-enrichment with pre-treatment using PrP^C-specific aptamers, to remove normal prions from a sample, could be applied as diagnostic tools in double ligand assay systems.[17] Such an enrichment method of PrP^{Sc} might be required for early stage detection of the β form PrP because it exists in extremely low proportions compared to the α form. After treatment with PrP^C-specific ligands, apt #1 may be useful for PrP^{Sc} enrichment, rather than employing an antibody without PK treatment.

In a recent publication investigating the interaction between RNAs and recombinant PrP, it was shown that PrP aggregates could be induced by the presence of small synthetic oligonucleotides and aggregates with total RNA extract from cultured mouse neuroblastoma cells (N2a) were cytotoxic.[39] A sensitive method of pathological prion protein detection using cyclic amplification of protein misfolding (PMCA) has been developed.[41] It has been reported that successful PMCA propagation of PrP^{Sc} molecules in a purified system requires accessory poly (A) RNA molecules.[42] Association with PrP and some specific RNAs such as RNA aptamers might help in this field.

In conclusion, we succeeded in harvesting an RNA aptamer against bPrP and bPrP-β, and in producing a high affinity, and a 17 mer minimized form containing 5 adenines at the 5'-site of $(GGA)_4$. Its ability to bind to bPrP (102–241), which corresponds to PrP 27–30, indicates that it may detect PK-digested PrP as well as antibodies. These aptamers will, we believe, be valuable in the study of conversions, diagnosis and therapy of prion disease.

Materials and Methods

Proteins. Recombinant bPrP (amino acids 25–241), amyloidogenic PrP prepared from recombinant bPrP (bPrP-β) and truncated bPrPs [bPrP (102–241): amino acids 102–241; bPrP (132–241): amino acids 132–241] were purchased from Alicon (Switzerland).

In vitro selection of RNA aptamers against bPrP. An N55S RNA pool containing a region of 55 randomized nucleotide [5'-GGGAGGUGGAACUGAAGGAGA-(N55)-ACUUCGCAAUCGCUCUACGCA-3'] was used to perform in vitro selection on a 0.45 μm HAWP nitrocellulose filter (Millipore). RNAs were heat denatured at 90°C for 2 min, 72°C for 5 min, 55°C for 5 min, 37°C for 2 min and cooled to room temperature in 50 μl of binding buffer [20 mM Tris-HCl (pH 7.5) and 100 mM NaCl] prior to use. The RNA pool was incubated for 10 to 30 min with bPrP in the presence of competitor RNAs (tRNA and/or anti-mPrP aptamer 60–3,[16] at room temperature. This mixed solution was passed through the nitrocellulose filter and washed with the binding buffer. RNA bound to bPrP on the filter was recovered with 400 μl of 7 M urea at 90°C for 5 min. The eluted RNA was ethanol precipitated and reverse transcribed using AMV reverse transcriptase (Wako) at 42°C for 1 h. The product was PCR amplified (94°C for 30 sec, 55°C for 30 sec and 72°C for 30 sec) using Gene Taq (Nippon Gene) with forward primer [5'-TGTAATACGACTCACTATAGG GAGGTGGAACTGAAGGAGA-3'] and reverse primer [5'-TGC GTAGAGCGATTGCGAAGT-3'] (Fasmac), and transcribed using the T7 Ampliscribe Kit (Epicentre Technologies). The RNA product was treated with DNase I and purified by Micro Bio-Spin Columns P-30 (Bio-Rad) or 8% PAGE containing 7 M urea and subjected to the next round of selection. From the eighth round of selection mutagenic PCR[21] was introduced. After the tenth generation cDNA pool was inserted into the pGEM-T Easy vector (Promega), cloned in *Escherichia coli* JM109 strain, and sequenced (ABI 3100; Applied Biosystems).

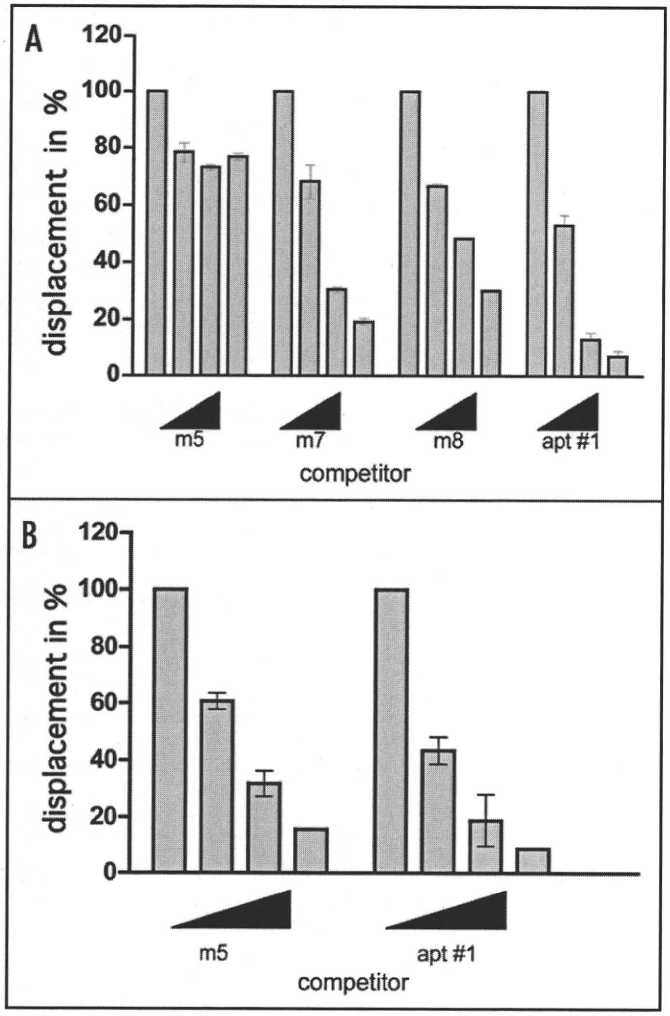

Figure 5. Comparison of binding of apt #1 and bPrP using competitive binding assay. The #1 mutants (m7, m8) contained substitutions (shown underlined) in the conserved region $(GGA)_4$ as follows: m7: 5'-GGUGGAGGAGGA-3'; m8: 5'-GGUGGUGGUGGU-3'. The competitor RNAs were added in various concentrations with 0, 1, 5 and 10-fold greater molar concentrations of labeled apt #1. Binding assay was performed in the presence of 10 mM KCl (A) and in the absence of KCl (B).

Preparation of RNA aptamer. To prepare RNA aptamer, the double-stranded DNA generated by PCR was used as a template for in vitro transcription by T7 RNA polymerase, as described above.

Mutant RNAs of apt #1 were prepared from mutagenic PCR using the following DNA templates (Fasmac) and the selection primers: for m1 [5'-TGC GTA GAG CGA TTG CGA AGT TGC TCA UCC UCC UCC TCT TGG GCT ACT TCC TCA TTC GAG AGA TGA ATG GAT TGT CTC CTT CAG TTC CAC CT CCC-3']; for m2 [5'-TGC GTA GAG CGA TTG CGA AGT TGC TCA UCC UCC TCT TGG GCT ACT TCC TCA TTC GAG AGA TGA ATG GAT TGT CTC CTT CAG TTC CAC CTC CC-3']; for m3 [5'-TGC GTA GAG CGA TTG CGA AGT TGC TCA TCT TGG GCT ACT TCC TCA TTC GAG AGA TGA ATG GAT TGT CTC CTT CAG TTC CAC CTC CC-3']; for m4 [5'-TGC GTA GAG CGA TTG CGA AGT TGC TCA AAA AAA AAA AAA TCT TGG GCT ACT TCC TCA TTC GAG AGA TGA ATG GAT TGT CTC CTT CAG TTC CAC CTC CC-3']; for m5 [5'-TGC GTA GAG CGA TTG CGA AGT TGC TCA TUU TUU TUU TUU TCT TGG GCT ACT TCC TCA TTC GAG AGA TGA ATG GAT TGT CTC CTT CAG TTC CAC CTC CC-3']; for m7 [5'-TGC GTA GAG CGA TTG CGA AGT TGC TCA TCC TCC TCC ACC TCT TGG GCT ACT TCC TCA TTC GAG AGA TGA ATG GAT TGT CTC CTT CAG TTC CAC CTC CC-3']; for m8 [5'-TGC GTA GAG CGA TTG CGA AGT TGC TCA ACC ACC ACC ACC TCT TGG GCT ACT TCC TCA TTC GAG AGA TGA ATG GAT TGT CTC CTT CAG TTC CAC CTC CC-3']. To prepare C#1, the generated PCR fragment using plasmid #1 as template and the proper primers (+) c#1 and (-) c#1, were used for in vitro transcription by T7 RNA polymerase as described above. (+) c#1: [5'-TGT AAT ACG ACT CAC TAT AGG CGT AGA GCG ATT GCG AAG-3']; and (-) c#1: [5'-GGG AGG TGG AAC TGA AGG AGA-3'].

Table 4 **Comparison of binding affinities for bPrP and bPrP-β between GGA repeat containing RNAs and DNA**

RNA/DNA	sequence	K_d (nM)	
		bPrP	bPrP-β
apt #1	-	31 ± 6	220 ± 70
$r(GGA)_4$	r(GGAGGAGGAGGA)	8.5 ± 3.4	280 ± 80
$d(GGA)_4$	d(GGAGGAGGAGGA)	64 ± 31	≥1000
R14	r(GGAGGUUUUGGAGG)	32 ± 18	610 ± 240

The chemically synthesized RNAs or DNAs: $r(GGA)_4$-15, $r(GGA)_4$, $d(GGA)_4$, R14, $r(GGA)_4$-16, $r(GGA)_4$-17, $r(GGA)_4$-18 and $r(GGA)_4$-19 were purchased from Fasmac (Japan). 5'-biotinylated RNAs (Bi#1, BiC#1) were prepared with a 5' end tag nucleic acid labeling system (Vector Laboratories).

Binding assay of anti-bPrP aptamer. Radioisotope labeling of RNA by in vitro transcription was carried out using α-^{32}P-ATP, as previously described.[16] Refolded ^{32}P labeled aptamer (10 nM) was mixed with varying concentrations of bPrP, or its derivatives, to a total volume of 25 μl in reaction buffer [20 mM Tris-HCl (pH 7.5), 100 mM NaCl or 10 mM KCl]. After 20 min incubation, the mixture was passed through a nitrocellulose filter and washed with 500 μl of the reaction buffer. The amount of bound RNA was measured with BAS 2500 (Fuji Film), and binding activities were calculated as the percentage of input RNA retained on the filter in the protein-RNA complex. We determined the equilibrium dissociation constant (K_d) using GraphPad PRISM using non-linear regression curve fitting, and a one site binding hyperbola equation (RNA binding (%) = B_{max} x [PrP]/(K_d + [PrP]), where B_{max} is the maximum bound at saturating PrP concentrations).

Northwestern assay with the aptamer. The Northwestern assay was performed using conventional methods.[22] A sample of 10 μl 10% bovine brain homogenate in suspension buffer [0.1% Nonidet P-40, 0.1% deoxycholate, 20 mM Tris-HCl (pH 7.5) and 100 mM NaCl] was separated by 10% SDS-PAGE and transferred to a 0.22 μm nitrocellulose membrane (Bio-Rad). A sample of 2 ml 1% BSA in binding buffer [20 mM Tris-HCl (pH 7.5) and 10 mM KCl] was used for blocking for 30 min. Proceeding this were 30 min incubation, with 200 nM of 5'-biotin labeled apt #1

Table 5 Comparison of adenine stretch at 5'-site of $(GGA)_4$ with binding affinities of bPrP, bPrP(102-241) and bPrP-β

aptamers	sequence	K_d (nM) bPrP	bPrP (102-241)	bPrP-β
r$(GGA)_4$-19	AAAAAAAGGAGGAGGAGGA	17 ± 5	540 ± 310	270 ± 90
r$(GGA)_4$-18	AAAAAAGGAGGAGGAGGA	10 ± 2	160 ± 50	150 ± 40
r$(GGA)_4$-17	AAAAAGGAGGAGGAGGA	9.4 ± 4.0	270 ± 120	78 ± 30
r$(GGA)_4$-16	AAAAGGAGGAGGAGGA	16 ± 3	190 ± 50	92 ± 26
r$(GGA)_4$-15	AAA GGAGGAGGAGGA	16 ± 4	220 ± 90	200 ± 90
r$(GGA)_4$	GGAGGAGGAGGA	8.5 ± 3.4	240 ± 90	280 ± 80

(Bi#1) in binding buffer, followed by a 30 min incubation with streptavidin-alkaline phosphatase conjugate (SA-AP; 2 ng/μl; Roche Applied Science) in binding buffer and a 1 min incubation with CDP-Star (20 mg/ml, Roche Applied Science). Detection was carried out using ECL Mini-Camera (Amersham Biosciences) and Polaroid film. For the standard immuno-blotting assay of $bPrP^C$, a T2 antibody was used.[23] All procedures were performed at room temperature.

Dot-blotting assay. 5' biotinylated RNA, Bi#1 or BiC#1, was spotted on nitrocellulose membrane and UV cross-linked for 5 min. Different amounts of bPrP (480, 240, 120, 60 and 30 ng) were spotted and air-dried for 10 min. The membrane was treated by blocking with 1 % BSA in reaction buffer [20 mM Tris-HCl (pH 7.5), 10 mM KCl] for 30 min, incubating with 200 nM of Bi#1 or BiC#1 in the presence of poly U (0.5 μg/μl, Amersham Biosciences) for 20 min, and then incubating with SA-AP (2 ng/μl) in reaction buffer for 30 min. Following a 1 min incubation with CDP-Star (20 mg/ml) in 0.1 M Tris-HCl (pH 9.5), detection was carried out with ECL Mini-Camera and Polaroid film. All procedures were performed at room temperature.

Circular dichroism spectroscopy. CD spectra were recorded with a JASCO J-720 Spectropolarimeter (JASCO) as previously reported.[24] A cell of 1 mm light path length and 300 μl volume was used to analyze in titration with KCl (0, 1, 10, 100 mM). The spectra were scanned four times from 200 nm to 330 nm. The CD intensities were expressed in [θ] per residue.

Competitive binding assay against bPrP. To characterize the specific binding of apt #1, binding of apt #1 to bPrP with increasing concentrations of competitor RNAs or DNAs were measured using a filter-binding assay. The labeled apt #1 (25 nM) was incubated with bPrP (50 nM) in the presence of a competitor (0, 1, 5 and 10-fold molar ratios) in binding buffer [20 mM Tris-HCl (pH 7.5), 10 mM KCl] for 20 min. The mixture was passed through a nitrocellulose filter, washed with 500 μl binding buffer, and the amount of binding of labeled apt #1 was determined as described above. 100% maximal binding is defined as the percentage of apt #1 bound to bPrP in the absence of any competitor.

Acknowledgements

The authors thank Drs. Katahira and Matsugami of Yokohama City University for measurement of CD spectra and helpful discussions. This work was supported by the fund from National Institute of Advanced Industrial Science and Technology (to S.N.) and by Grant-in-Aid from the BSE Control Project of the Ministry of Agriculture, Forestry and Fisheries of Japan (to T.Y.).

References

1. Pan KM, Baldwin M, Nguyen J, Gasset M, Serban A, Groth D, Mehlhorn I, Huang Z, Fletterick RJ, Cohen FE, et al. Conversion of alpha-helices into beta-sheets features in the formation of the scrapie prion proteins. Proc Natl Acad Sci USA 1993; 90:10962-6.
2. Prusiner SB. Prions. Proc Natl Acad Sci USA 1998; 95:13363-83.
3. Marc D, Mercey R, Lantier F. Scavenger, transducer, RNA chaperone? What ligands of the prion protein teach us about its function. Cell Mol Life Sci 2007; 64:815-29.
4. Wadsworth JD, Collinge J. Update on human prion disease. Biochim Biophys Acta 2007; 1772:598-609.
5. Hu W, Kieseier B, Frohman E, Eagar TN, Rosenberg RN, Hartung HP, Stuve O. Prion proteins: physiological functions and role in neurological disorders. J Neurol Sci 2008; 264:1-8.
6. Ellington AD, Szostak JW. In vitro selection of RNA molecules that bind specific ligands. Nature 1990; 346:818-22.
7. Tuerk C, Gold L. Systematic evolution of ligands by exponential enrichment: RNA ligands to bacteriophage T4 DNA polymerase. Science 1990; 249:505-10.
8. Yang Y, Yang D, Schluesener HJ, Zhang Z. Advances in SELEX and application of aptamers in the central nervous system. Biomol Eng 2007; 24:583-92.
9. Mairal T, Ozalp VC, Lozano Sanchez P, Mir M, Katakis I, O'Sullivan CK. Aptamers: molecular tools for analytical applications. Anal Bioanal Chem 2008; 390:989-1007.
10. Weiss S, Proske D, Neumann M, Groschup MH, Kretzschmar HA, Famulok M, Winnacker EL. RNA aptamers specifically interact with the prion protein PrP. J Virol 1997; 71:8790-7.
11. Proske D, Gilch S, Wopfner F, Schatzl HM, Winnacker EL, Famulok M. Prion-protein-specific aptamer reduces PrP^{Sc} formation. Chembiochem 2002; 3:717-25.
12. Rhie A, Kirby L, Sayer N, Wellesley R, Disterer P, Sylvester I, Gill A, Hope J, James W, Tahiri-Alaoui A. Characterization of 2'-fluoro-RNA aptamers that bind preferentially to disease-associated conformations of prion protein and inhibit conversion. J Biol Chem 2003; 278:39697-705.
13. Sayer NM, Cubin M, Rhie A, Bullock M, Tahiri-Alaoui A, James W. Structural determinants of conformationally selective, prion-binding aptamers. J Biol Chem 2004; 279:13102-9.
14. Sekiya S, Nishikawa F, Noda K, Kumar PK, Yokoyama T, Nishikawa S. In vitro selection of RNA aptamers against cellular and abnormal isoform of mouse prion protein. Nucleic Acids Symp Ser (Oxf) 2005; 361-2.
15. Mercey R, Lantier I, Maurel MC, Grosclaude J, Lantier F, Marc D. Fast, reversible interaction of prion protein with RNA aptamers containing specific sequence patterns. Arch Virol 2006; 151:2197-214.
16. Sekiya S, Noda K, Nishikawa F, Yokoyama T, Kumar PK, Nishikawa S. Characterization and application of a novel RNA aptamer against the mouse prion protein. J Biochem 2006; 139:383-90.
17. Takemura K, Wang P, Vorberg I, Surewicz W, Priola SA, Kanthasamy A, Pottathil R, Chen SG, Sreevatsan S. DNA aptamers that bind to PrP(C) and not PrP(Sc) show sequence and structure specificity. Exp Biol Med (Maywood) 2006; 231:204-14.
18. Nishikawa F, Murakami K, Noda K, Yokoyama T, Nishikawa S. Detection of structural changes of RNA aptamer containing GGA repeats under the ionic condition using the microchip electrophoresis. Nucleic Acids Symp Ser (Oxf) 2007; 397-8.
19. Bibby DF, Gill AC, Kirby L, Farquhar CF, Bruce ME, Garson JA. Application of a novel in vitro selection technique to isolate and characterise high affinity DNA aptamers binding mammalian prion proteins. J Virol Methods 2008; 151:107-15.
20. Ogasawara D, Hasegawa H, Kaneko K, Sode K, Ikebukuro K. Screening of DNA Aptamer Against Mouse Prion Protein by Competitive Selection. Prion 2008; 1:248-54.
21. Fromant M, Blanquet S, Plateau P. Direct random mutagenesis of gene-sized DNA fragments using polymerase chain reaction. Anal Biochem 1995; 224:347-53.
22. Bagga PS, Wilusz J. Northwestern screening of expression libraries. Methods Mol Biol 1999; 118:245-56.
23. Hayashi H, Takata M, Iwamaru Y, Ushiki Y, Kimura KM, Tagawa Y, Shinagawa M, Yokoyama T. Effect of tissue deterioration on postmortem BSE diagnosis by immunobiochemical detection of an abnormal isoform of prion protein. J Vet Med Sci 2004; 66:515-20.
24. Matsugami A, Ouhashi K, Kanagawa M, Liu H, Kanagawa S, Uesugi S, Katahira M. An intramolecular quadruplex of (GGA)(4) triplet repeat DNA with a G:G:G:G tetrad and a G(:A):G(:A):G(:A):G heptad, and its dimeric interaction. J Mol Biol 2001; 313:255-69.

25. Laughlan G, Murchie AI, Norman DG, Moore MH, Moody PC, Lilley DM, Luisi B. The high-resolution crystal structure of a parallel-stranded guanine tetraplex. Science 1994; 265:520-4.
26. Davis JT. G-quartets 40 years later: from 5'-GMP to molecular biology and supramolecular chemistry. Angew Chem Int Ed Engl 2004; 43:668-98.
27. Balagurumoorthy P, Brahmachari SK, Mohanty D, Bansal M, Sasisekharan V. Hairpin and parallel quartet structures for telomeric sequences. Nucleic Acids Res 1992; 20:4061-7.
28. Catasti P, Chen X, Moyzis RK, Bradbury EM, Gupta G. Structure-function correlations of the insulin-linked polymorphic region. J Mol Biol 1996; 264:534-45.
29. Nandi PK. Interaction of prion peptide HuPrP106-126 with nucleic acid. Arch Virol 1997; 142:2537-45.
30. Nandi PK, Nicole JC. Nucleic acid and prion protein interaction produces spherical amyloids which can function in vivo as coats of spongiform encephalopathy agent. J Mol Biol 2004; 344:827-37.
31. Liu H, Kugimiya A, Matsugami A, Katahira M, Uesugi S. Quadruplex structures of RNA 14-mer, r(GGAGGUUUUGGAGG) and DNA 14-mer, d(GGAGGTTTTGGAGG). Nucleic Acids Res Suppl 2002; 2:177-8.
32. Zeiler B, Adler V, Kryukov V, Grossman A. Concentration and removal of prion proteins from biological solutions. Biotechnol Appl Biochem 2003; 37:173-82.
33. Prusiner SB, McKinley MP, Bowman KA, Bolton DC, Bendheim PE, Groth DF, Glenner GG. Scrapie prions aggregate to form amyloid-like birefringent rods. Cell 1983; 35:349-58.
34. Prusiner SB, Groth DF, Bolton DC, Kent SB, Hood LE. Purification and structural studies of a major scrapie prion protein. Cell 1984; 38:127-34.
35. Caughey B, Raymond GJ, Ernst D, Race RE. N-terminal truncation of the scrapie-associated form of PrP by lysosomal protease(s): implications regarding the site of conversion of PrP to the protease-resistant state. J Virol 1991; 65:6597-603.
36. Prusiner SB, McKinley MP, Groth DF, Bowman KA, Mock NI, Cochran SP, Masiarz FR. Scrapie agent contains a hydrophobic protein. Proc Natl Acad Sci USA 1981; 78:6675-9.
37. Luhrs T, Zahn R, Wuthrich K. Amyloid formation by recombinant full-length prion proteins in phospholipid bicelle solutions. J Mol Biol 2006; 357:833-41.
38. Riek R, Hornemann S, Wider G, Glockshuber R, Wuthrich K. NMR characterization of the full-length recombinant murine prion protein, mPrP(23-231). FEBS Lett 1997; 413:282-8.
39. Gomes MP, Millen TA, Ferreira PS, Cunha ESNL, Vieira TC, Almeida MS, Silva JL, Cordeiro Y. Prion protein complexed to N2a cellular RNAs through its N-terminal domain forms aggregates and is toxic to murine neuroblastoma cells. J Biol Chem 2008; 283:19616-25.
40. Davidowitz E, Eljuga L, Dover K, Tian J, Grossman A. Concentration of prion protein from biological samples to increase the limits of detection by immunoassay. Biotechnol Appl Biochem 2005; 41:247-53.
41. Saborio GP, Permanne B, Soto C. Sensitive detection of pathological prion protein by cyclic amplification of protein misfolding. Nature 2001; 411:810-3.
42. Deleault NR, Harris BT, Rees JR, Supattapone S. Formation of native prions from minimal components in vitro. Proc Natl Acad Sci USA 2007; 104:9741-6.

JOURNAL OF BACTERIOLOGY, May 2008, p. 3613–3621 Vol. 190, No. 10
0021-9193/08/$08.00+0 doi:10.1128/JB.01850-07

Structural Analysis and Biosynthesis Gene Cluster of an Antigenic Glycopeptidolipid from *Mycobacterium intracellulare*▽†

Nagatoshi Fujiwara,[1]* Noboru Nakata,[2] Takashi Naka,[1,3] Ikuya Yano,[3] Matsumi Doe,[4] Delphi Chatterjee,[5] Michael McNeil,[5] Patrick J. Brennan,[5] Kazuo Kobayashi,[6] Masahiko Makino,[2] Sohkichi Matsumoto,[1] Hisashi Ogura,[7] and Shinji Maeda[8]

Department of Host Defense[1] and Virology,[7] Osaka City University Graduate School of Medicine, Osaka 545-8585, Japan; Department of Microbiology, Leprosy Research Center, National Institute of Infectious Diseases, Tokyo 189-0002, Japan[2]; Japan BCG Laboratory, Tokyo 204-0022, Japan[3]; Department of Chemistry, Graduate School of Science, Osaka City University, Osaka 558-8585, Japan[4]; Department of Microbiology, Immunology and Pathology, Colorado State University, Colorado 80523[5]; Department of Immunology, National Institute of Infectious Diseases, Tokyo 162-8640, Japan[6]; and Molecular Epidemiology Division, Mycobacterium Reference Center, The Research Institute of Tuberculosis, Japan Anti-Tuberculosis Association, Tokyo 204-8533, Japan[8]

Received 24 November 2007/Accepted 1 March 2008

***Mycobacterium avium-Mycobacterium intracellulare* complex (MAC) is the most common isolate of nontuberculous mycobacteria and causes pulmonary and extrapulmonary diseases. MAC species can be grouped into 31 serotypes by the epitopic oligosaccharide structure of the species-specific glycopeptidolipid (GPL) antigen. The GPL consists of a serotype-common fatty acyl peptide core with 3,4-di-*O*-methyl-rhamnose at the terminal alaninol and a 6-deoxy-talose at the *allo*-threonine and serotype-specific oligosaccharides extending from the 6-deoxy-talose. Although the complete structures of 15 serotype-specific GPLs have been defined, the serotype 16-specific GPL structure has not yet been elucidated. In this study, the chemical structure of the serotype 16 GPL derived from *M. intracellulare* was determined by using chromatography, mass spectrometry, and nuclear magnetic resonance analyses. The result indicates that the terminal carbohydrate epitope of the oligosaccharide is a novel *N*-acyl-dideoxy-hexose. By the combined linkage analysis, the oligosaccharide structure of serotype 16 GPL was determined to be 3-2′-methyl-3′-hydroxy-4′-methoxy-pentanoyl-amido-3,6-dideoxy-β-hexose-(1→3)-4-*O*-methyl-α-L-rhamnose-(1→3)-α-L-rhamnose-(1→3)-α-L-rhamnose-(1→2)-6-deoxy-α-L-talose. Next, the 22.9-kb serotype 16-specific gene cluster involved in the glycosylation of oligosaccharide was isolated and sequenced. The cluster contained 17 open reading frames (ORFs). Based on the similarity of the deduced amino acid sequences, it was assumed that the ORF functions include encoding three glycosyltransferases, an acyltransferase, an aminotransferase, and a methyltransferase. An *M. avium* serotype 1 strain was transformed with cosmid clone no. 253 containing *gtfB-drrC* of *M. intracellulare* serotype 16, and the transformant produced serotype 16 GPL. Together, the ORFs of this serotype 16-specific gene cluster are responsible for the biosynthesis of serotype 16 GPL.**

Mycobacterial diseases, such as tuberculosis and infection due to nontuberculous mycobacteria (NTM), are still among the most serious infectious diseases in the world. The incidence is increasing because of the spread of drug-resistant mycobacteria and the human immunodeficiency virus (HIV) infection/AIDS epidemic (16, 17, 30). *Mycobacterium avium-Mycobacterium intracellulare* complex (MAC) is the most common among isolates of NTM and is distributed ubiquitously in the environment. MAC causes pulmonary and extrapulmonary diseases in both immunocompromised and immunocompetent hosts. It affects primarily patients with advanced HIV infection. MAC includes at least two mycobacterial species, *M. avium* and *M. intracellulare*, that cannot be differentiated on the basis of traditional physical and biochemical tests (1, 41).

The cell envelope of mycobacteria is a complex and unusual structure. The key feature of this structure is an extraordinarily high lipid concentration (6, 10). To better understand the pathogenesis of MAC infection, it is necessary to elucidate the molecular structure and biochemical features of the lipid components. Among MAC lipids, the glycopeptidolipid (GPL) is of particular importance, because it shows not only serotype-specific antigenicity but also immunomodulatory activities in the host immune responses (2, 9, 23). Structurally, GPLs are composed of two parts, a tetrapeptide-amino alcohol core and a variable oligosaccharide (OSE). C_{26}-C_{34} fatty acyl-D-phenylalanine-D-*allo*-threonine-D-alanine-L-alaninol (D-Phe-D-*allo*-Thr-D-Ala-L-alaninol) is further linked with 6-deoxy talose (6-d-Tal) and 3,4-di-*O*-methyl rhamnose (3,4-di-*O*-Me-Rha) at D-*allo*-Thr and the terminal L-alaninol, respectively. This type of core GPL is found in all subspecies of MAC, shows a common antigenicity, and is further glycosylated at 6-d-Tal to form a serotype-specific OSE.

At present, 31 distinct serotype-specific GPLs have been identified serologically and chromatographically (9). Although the standard technique for differentiation of MAC subspecies

* Corresponding author. Mailing address: Department of Host Defense, Osaka City University Graduate School of Medicine, 1-4-3 Asahi-machi, Abeno-ku, Osaka 545-8585, Japan. Phone: 81 6 6645 3746. Fax: 81 6 6645 3747. E-mail: fujiwara@med.osaka-cu.ac.jp.

† Supplemental material for this article may be found at http://jb.asm.org/.

▽ Published ahead of print on 7 March 2008.

has been serotyping based on the OSE residue of its GPL, the complete structures of only 15 GPLs have been defined. In addition to the chemical structures of various GPLs, genes encoding the glycosylation pathways in the biosynthesis of GPL have been identified and characterized (12, 21, 31). Epidemiological studies have shown that MAC serotypes 4 and 8 are the most frequently isolated from patients, and MAC serotype 16 is one of the next most common groups (32, 40). It has been suggested that the serotypes of MAC isolates participate in their virulence (29), and thus, understanding of the structure-pathogenicity relationship of GPLs is necessary. In the present study, we demonstrate the complete OSE structure of the GPL derived from serotype 16 MAC (*M. intracellulare*), which has a unique terminal-acylated-amido sugar, and we characterized the serotype 16 GPL-specific gene cluster involved in the glycosylation of carbohydrates.

MATERIALS AND METHODS

Bacterial strains and preparation of GPL. *M. intracellulare* serotype 16 strain ATCC 13950^T (NF 115) was purchased from the American Type Culture Collection (Manassas, VA). Three clinical isolates of *M. intracellulare* serotype 16 (NF 116 and 117) and *M. avium* serotype 1 (NF 113) were maintained in The Research Institute of Tuberculosis, Japan Anti-Tuberculosis Association. The preparation of GPL was performed as described previously (18, 24, 26). Briefly, each strain of *M. intracellulare* serotype 16 was grown in Middlebrook 7H9 broth (Difco Laboratories, Detroit, MI) with 0.5% glycerol and 10% Middlebrook oleic acid-albumin-dextrose-catalase enrichment (Difco) at 37°C for 2 to 3 weeks. The heat-killed bacteria were sonicated, and crude lipids were extracted with chloroform-methanol (2:1, vol/vol). The extracted lipids were dried and hydrolyzed with 0.2 N sodium hydroxide in methanol at 37°C for 2 h. After neutralization with 6 N hydrochloric acid, alkaline-stable lipids were partitioned by a two-layer system of chloroform-methanol (2:1, vol/vol) and water. The organic phase was recovered, evaporated, and precipitated with acetone to remove any acetone-insoluble components containing phospholipids and glycolipids. The supernatant was collected by centrifugation, dried, and then treated with a Sep-Pak silica cartridge (Waters Corporation, Milford, MA) with washing (chloroform-methanol, 95:5, vol/vol) and elution (chloroform-methanol, 1:1, vol/vol) for partial purification. GPL was completely purified by preparative thin-layer chromatography (TLC) of Silica Gel G (20 by 20 cm, 250 μm; Uniplate; Analtech, Inc., Newark, DE). The TLC plate was repeatedly developed with chloroform-methanol-water (65:25:4 and 60:16:2, vol/vol/vol) until a single spot was obtained. After exposure of the TLC plate to iodine vapor, the GPL band was marked, and then, the silica gels were scraped off and the GPL was eluted with chloroform-methanol (2:1, vol/vol).

Preparation of OSE moiety. β elimination of GPL was performed with alkaline borohydride, and the OSE elongated from D-*allo*-Thr was released as described previously (18, 24). Briefly, the GPL was dissolved in ethanol, and an equal volume of 10 mg/ml sodium borohydride or borodeuteride in 0.5 N sodium hydroxide was added and then stirred at 60°C for 16 h. The reaction mixture was decationized with Dowex 50W-X8 beads (Dow Chemical Company, Midland, MI), collected, and evaporated under nitrogen to remove boric acid. The dried residue was partitioned in two layers of chloroform-methanol (2:1, vol/vol) and water. The upper aqueous phase was recovered and evaporated. In these processes, the serotype 16-specific OSE was purified as an oligoglycosyl alditol.

MALDI-TOF and MALDI-TOF/TOF MS analyses. The molecular species of the intact GPL was detected by matrix-assisted laser desorption ionization–time of flight mass spectrometry (MALDI-TOF MS) with an Ultraflex II (Bruker Daltonics, Billerica, MA). The GPL was dissolved in chloroform-methanol (2:1, vol/vol) at a concentration of 1 mg/ml, and 1 μl was applied directly to the sample plate, and then 1 μl of 10 mg/ml 2,5-dihydroxybenzoic acid in chloroform-methanol (1:1, vol/vol) was added as a matrix. The intact GPL was analyzed in the reflectron mode with an accelerating voltage operating in a positive mode of 20 kV (5). Then the fragment pattern of the OSE was analyzed with MALDI-TOF/TOF MS. The OSE was dissolved in ethanol-water (3:7, vol/vol), and the matrix was 10 mg/ml 2,5-dihydroxybenzoic acid in ethanol-water (3:7, vol/vol). The OSE and the matrix were applied to the sample plate according to the method for intact GPL and analyzed in the lift-lift mode.

GC and GC-MS analyses of carbohydrates and *N*-acylated short-chain fatty acid. To determine the glycosyl composition and linkage position, gas chromatography (GC) and GC-MS analyses of partially methylated alditol acetate derivatives were performed. Perdeuteromethylation was conducted by the modified procedure of Hakomori as described previously (18, 20). Briefly, the dried OSE was dissolved with a mixture of dimethyl sulfoxide and sodium hydroxide, and deuteromethyl iodide was added. The reaction mixture was stirred at room temperature for 15 min and then water and chloroform were added. The chloroform-containing perdeuteromethylated OSE layer was collected, washed with water two times, and then completely evaporated. Partially deuteromethylated alditol acetates were prepared from perdeuteromethylated OSE by hydrolysis with 2 N trifluoroacetic acid at 120°C for 2 h, reduction with 10 mg/ml sodium borodeuteride at 25°C for 2 h, and acetylation with acetic anhydride at 100°C for 1 h (8, 18, 25). To identify amino-linked fatty acids, acidic methanolysis of serotype 16 GPL was performed with 1.25 M hydrogen chloride in methanol (Sigma-Aldrich, St. Louis, MO) at 100°C for 90 min, and the fatty acid methyl esters were extracted with *n*-hexane under the cooled ice. GC was performed using a 5890 series II gas chromatograph (Hewlett Packard, Avondale, PA) equipped with a fused SPB-1 capillary column (30 m, 0.25-mm inner diameter; Supelco Inc., Bellefonte, PA). Helium was used for electron impact (EI)-MS and isobutane for chemical ionization (CI)-MS as a carrier gas. A JMS SX102A double-focusing mass spectrometer (JEOL, Tokyo, Japan) was connected to the gas chromatograph as a mass detector. The molecular separator and the ion source energy were 70 eV for EI and 30 eV for CI, and the accelerating voltage was 8 kV. The D and L configurations of Rha residues were determined by comparative GC-MS analysis of trimethylsilylated (*S*)-(+)-sec-butyl glycosides and (*R*)-(−)-sec-butyl glycosides prepared from an authentic standard L-Rha (19).

NMR analysis of GPL. The GPL was dissolved in chloroform-d ($CDCl_3$)-methanol-d_4 (CD_3OD) (2:1, vol/vol). To define the anomeric configurations of each glycosyl residue, ^1H and ^{13}C nuclear magnetic resonance (NMR) was employed. Both homonuclear correlation spectrometry (COSY) and ^1H-detected [^1H, ^{13}C] heteronuclear multiple-quantum correlation (HMQC) were recorded with a Bruker Avance-600 (Bruker BioSpin Corp., Billerica, MA), as described previously (9, 18, 24, 34).

Construction of *M. intracellulare* serotype 16 cosmid library. A cosmid library of *M. intracellulare* serotype 16 strain ATCC 13950^T was constructed as described previously (18). Bacterial cells were disrupted mechanically, and genomic DNA was extracted with phenol-chloroform and then precipitated with ethanol. Genomic DNA randomly sheared into 30- to 50-kb fragments in the extraction process was fractionated and electroeluted from agarose gels using a Takara Recochip (Takara, Kyoto, Japan). These DNA fragments were rendered blunt ended using T4 DNA polymerase and deoxynucleoside triphosphates and then were ligated to dephosphorylated arms of pYUB412 (XbaI-EcoRV and EcoRV-XbaI), which were the kind gifts of William R. Jacobs, Jr. (Department of Microbiology and Immunology, Albert Einstein College of Medicine, Bronx, NY). The cosmid vector pYUB412 is an *Escherichia coli-Mycobacterium* shuttle vector with the *int-attP* sequence for integration into a mycobacterial chromosome, *oriE* for replication in *E. coli*, a hygromycin resistance gene, and an ampicillin resistance gene. After in vitro packaging using Gigapack III Gold extracts (Stratagene, La Jolla, CA), recombinant cosmids were introduced into *E. coli* STBL2 [F$^-$ *mcrA* Δ(*mcrBC-hsdRMS-mrr*) *recA1 endA1 lon gyrA96 thi supE44 relA1* l Δ(*lac-proAB*)] and stored at −80°C in 50% glycerol.

Isolation of cosmid clones carrying biosynthesis gene cluster of serotype 16 GPL and sequence analysis. Isolation of DNA from *E. coli* transductants was performed as described by Supply et al., with modifications (39). The colonies were picked, transferred to a 1.5-ml tube containing 50 μl of water, and then heated at 98°C for 5 min. After centrifugation at 14,000 rpm for 5 min, the supernatant was used as the PCR template. PCR was used to isolate cosmid clones carrying the rhamnosyltransferase (*rtfA*) gene with primers rtfA-F (5′-TTTTGGAGCGACGAGTTCATC-3′) and rtfA-R (5′-GTGTAGTTGACCACGCCGAC-3′). *rtfA* encodes an enzyme responsible for the transfer of Rha to 6-d-Tal in OSE (14, 31). The insert of cosmid clone no. 253 was sequenced using a BigDye Terminator, version 3.1, cycle sequencing kit (Applied Biosystems, Foster City, CA) and an ABI Prism 310 gene analyzer (Applied Biosystems). The putative function of each open reading frame (ORF) was identified by similarity searches between the deduced amino acid sequences and known proteins using BLAST (http://www.ncbi.nlm.nih.gov/BLAST/) and FramePlot (http://www.nih.go.jp/~jun/cgi-bin/frameplot.pl) with the DNASIS computer program (Hitachi Software Engineering, Yokohama, Japan).

Transformation of *M. avium* serotype 1 strain with cosmid clone no. 253. An *M. avium* serotype 1 strain (NF113) was transformed with pYUB412-cosmid clone no. 253 by electroporation, and hygromycin-resistant colonies were iso-

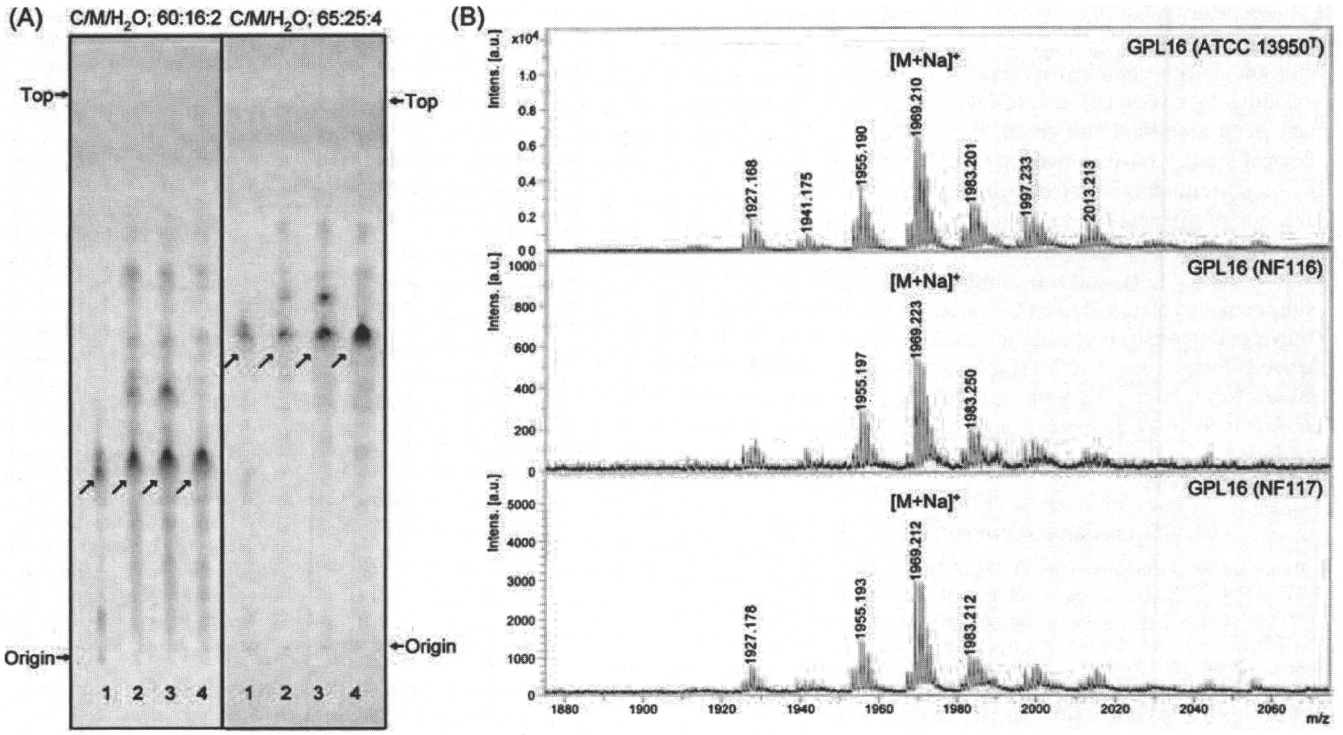

FIG. 1. TLC patterns and MALDI-TOF MS spectra of serotype 16 GPL. (A) Serotype 16 GPL purified from *M. intracellulare* ATCC 13950^T (NF 115) and the alkaline-stable lipids derived from ATCC 13950^T and two clinical isolates (NF 116 and 117) from left to right were developed on TLC plates with solvent systems of chloroform-methanol-water (65:25:4 and 60:16:2, vol/vol/vol). (B) The MALDI-TOF MS spectra were acquired using 10 mg/ml 2,5-dihydroxybenzoic acid in chloroform-methanol (1:1, vol/vol) as a matrix, and the molecularly related ions were detected as $[M+Na]^+$ in positive mode. Intens., intensity; a.u., absorbance units.

lated. Alkaline-stable lipids were prepared, and productive GPLs were examined by TLC and MALDI-TOF MS analyses.

Nucleotide sequence accession number. The nucleotide sequence reported here has been deposited in the NCBI GenBank database under accession no. AB355138.

RESULTS

Purification and molecular weight of intact GPL. Serotype 16 GPL from *M. intracellulare* ATCC 13950^T (NF 115) was detected as a spot by TLC, and the R_f values were 0.35 and 0.56 when developed with chloroform-methanol-water (60:16:2 and 65:25:4, vol/vol/vol, respectively). Two clinical isolates of *M. intracellulare*, NF 116 and 117, had serotype 16 GPLs that showed the same R_f values as the serotype 16 GPL derived from strain ATCC 13950^T. The serotype 16 GPL of *M. intracellulare* strain ATCC 13950^T was purified repeatedly by TLC and was shown as a single spot by TLC (Fig. 1A). The MALDI-TOF MS spectra of each serotype 16 GPL showed *m/z* 1969 for $[M+Na]^+$ as the main molecularly related ion in positive mode, with the homologous ions differing by 14 mass units at 1,955 and 1,983 (Fig. 1B). As a result, the main molecular weight of serotype 16 GPL was 1,946, which implied that it has a novel carbohydrate chain elongated from D-*allo*-Thr.

Carbohydrate composition of serotype 16 OSE. To determine the glycosyl compositions of serotype 16 OSE, alditol acetate derivatives of the serotype 16 GPL were analyzed by GC and GC-MS. The structurally defined serotype 4 GPL was used as a reference standard (9, 35). Comparison of the retention time and GC mass spectra (Fig. 2) with the alditol acetate derivatives of the serotype 16 GPL showed the presence of 3,4-di-*O*-Me-Rha, 4-*O*-Me-Rha, Rha, 6-d-Tal, and an unknown sugar residue (X1) in a ratio of approximately 1:1:2:1:1. The alditol acetate of X1 was eluted at a retention time of 29.3 min, greater than that of glucitol acetate on the SPB-1 column. The CI-MS spectrum of X1 was $[M+H]^+$ at *m/z* 520 as a parent ion and *m/z* 460 as a loss of 60 (acetate). The fragment ions of X1 sugar showed characteristic patterns in EI-MS. *m/z* 360 indicated the cleavage of C-3 and C-4, and *m/z* 300, 240, and 180 were fragmented with a loss of 60 (acetate). Similarly, *m/z* 374 indicated the cleavage of C-2 and C-3, and *m/z* 314 and 254 were fragmented with a loss of 60 (Fig. 3A and B). These results indicated that X1 was 3,6-dideoxy hexose (Hex). The odd molecular weight of X1, 519, and *m/z* 187, 127, and 59 implied the presence of one amido group esterified with a short-chain fatty acid, possibly. After methanolysis of serotype 16 GPL, the resultant fatty acid methyl esters were extracted carefully and analyzed by GC-MS. The EI-MS spectrum of a short-chain fatty acid methyl ester showed mass ions at *m/z* 176 ($[M]^+$), 145 ($[M-31]^+$), 117 ($[M-59]^+$), 99, 88, 85, and 59 (Fig. 3C) (33, 37). Taking the results together, X1 was structurally determined to be 3-2′-methyl-3′-hydroxy-4′-methoxy-pentanoyl-amido-3,6-dideoxy-Hex.

Glycosyl linkage and sequence of serotype 16 OSE. To determine the glycosyl linkage and sequence of the OSE, GC-MS of perdeuteromethylated alditol acetates and MALDI-TOF/TOF MS of the oligoglycosyl alditol from serotype 16 OSE

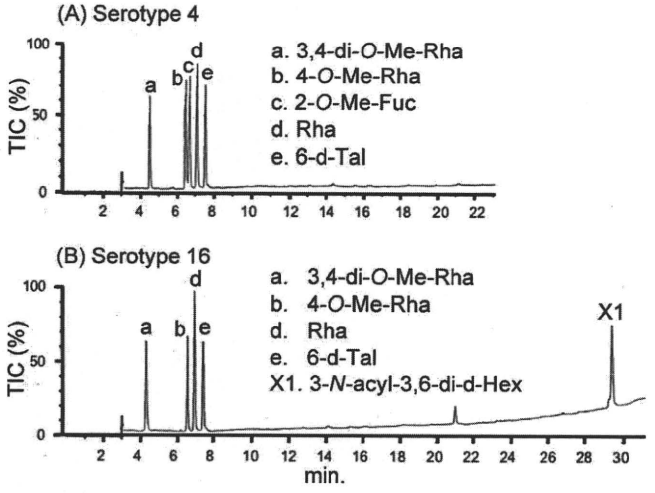

FIG. 2. Gas chromatograms of the alditol acetate derivatives from serotype 4 (A) and serotype 16 (B) GPLs. Total ion chromatograms (TIC) are shown. GC was performed on an SPB-1-fused silica column with a temperature program of 160°C for 2 min, followed by an increase of 4°C/min to 220°C, and holding at 220°C for 15 min. Comparison to the GC spectrum of serotype 4 GPL shows that serotype 16 GPL is composed of 3,4-di-*O*-Me-Rha, 4-*O*-Me-Rha, Rha, 6-d-Tal, and an unknown X1 sugar residue.

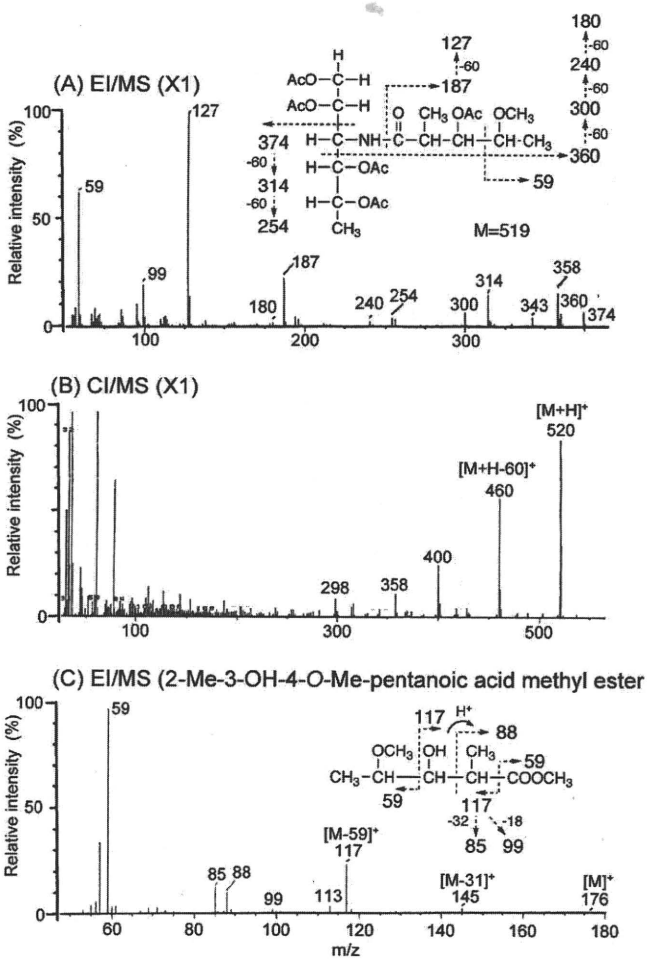

FIG. 3. EI-MS and CI-MS spectra of the alditol acetate derivative from X1 (A and B) and *N*-acylated-short-chain fatty acid methyl ester (C). The pattern of prominent fragment ions is illustrated. The CG column and condition were described in the legend for Fig. 2.

were performed. As shown in Fig. 4, the GC-MS spectra of perdeuteromethylated alditol acetates were assigned four major peaks, 1,3,4,5-tetra-*O*-deuteromethyl-2-*O*-acetyl-6-deoxy-talitol (*m/z* 109, 132, 154, 167, and 214); 2,4-di-*O*-deuteromethyl-1,3,5-tri-*O*-acetyl-rhamnitol (*m/z* 121, 134, 205, 240, and 253); 2-*O*-deuteromethyl-4-*O*-methyl-1,3,5-tri-*O*-acetyl-rhamnitol (*m/z* 121, 131, 202, and 237); and 2,4-di-*O*-deuteromethyl-1,5-di-*O*-acetyl-3-2′-methyl-3′-*O*-deuteromethyl-4′methoxy-pentanoyl-deuteromethylamido-3,6-dideoxy-hexitol (*m/z* 121, 134, and 341). These results revealed that the 6-d-Tal residue was linked at C-2; Rha and 4-*O*-Me-Rha were linked at C-1 and C-3; and the nonreducing terminus, 3-2′-methyl-3′-hydroxy-4′-methoxy-pentanoyl-amido-3,6-dideoxy-Hex, was C-1 linked. The MALDI-TOF/TOF MS spectrum of the oligoglycosyl alditol from serotype 16 OSE afforded the expected molecular ions $[M+Na]^+$ at *m/z* 931, together with the characteristic mass increments in the series of glycosyloxonium ions formed on fragmentation at *m/z* 312, 472, 618, and 764 from the terminal sugar *N*-acyl-Hex to 6-d-Tal and at *m/z* 336, 482, and 642 from 6-d-Tal to *N*-acyl-Hex (Fig. 5). Rha residues were determined to be in the L absolute configuration by comparative GC-MS analyses of trimethylsilylated (*S*)-(+)-sec-butyl glycosides and (*R*)-(−)-sec-butylglycosides (see Fig. S1 in the supplemental material). Taken together, these results established the sequence and linkage arrangement 3-2′-methyl-3′-hydroxy-4′-methoxy-pentanoyl-amido-3,6-dideoxy-Hex-(1→3)-4-*O*-Me-Rha-(1→3)-L-Rha-(1→3)-L-Rha-(1→2)-6-d-Tal, exclusively.

NMR analysis of serotype 16 OSE. The ^{1}H NMR and ^{1}H-^{1}H COSY analyses of the serotype 16 GPL revealed six distinct anomeric protons with corresponding H1-H2 cross peaks in the low field region at δ4.93, 4.92, 4.92, 4.84, 4.65 ($J_{1\text{-}2}$ = 2 to 3 Hz, indicative of α-anomers) and 4.51 (a doublet, $J_{1\text{-}2}$ = 7.7 Hz, indicative of a β-hexosyl unit). When further analyzed by ^{1}H-detected [^{1}H, ^{13}C] two-dimensional HMQC, the anomeric protons resonating at δ4.93, 4.92, 4.92, 4.84, 4.65, and 4.51 have C-1s resonating at δ101.57, 95.73, 101.40, 102.56, 100.97, and 103.36, respectively (for a summary, see Table S1 in the supplemental material). The J_{CH} values for each of these protons were calculated to be 171, 170, 171, 170, 169, and 161 Hz by measurement of the inverse-detection nondecoupled two-dimensional HMQC (Fig. 6). These results established that the terminal amido-Hex was a β configuration and the others were α-anomers.

Cloning and sequence of serotype 16 GPL biosynthesis cluster. To isolate the serotype 16 GPL biosynthesis cluster, the genomic cosmid library of *M. intracellulare* serotype 16 strain ATCC 13950^T was constructed. Primers were designed to amplify the region corresponding to the *rtfA* gene. More than 300 cosmid clones were tested using colony PCR with *rtfA* primers, and the positive clones no. 51 and 253 were isolated from the *E. coli* transductants. PCR analysis revealed that clone no. 253 contained a *drrC* gene but that clone no. 51 did not. Thus, we used clone no. 253 for subsequent sequence analysis for the *gtfB-drrC* region. The 22.9-kb region of *M. intracellulare* sero-

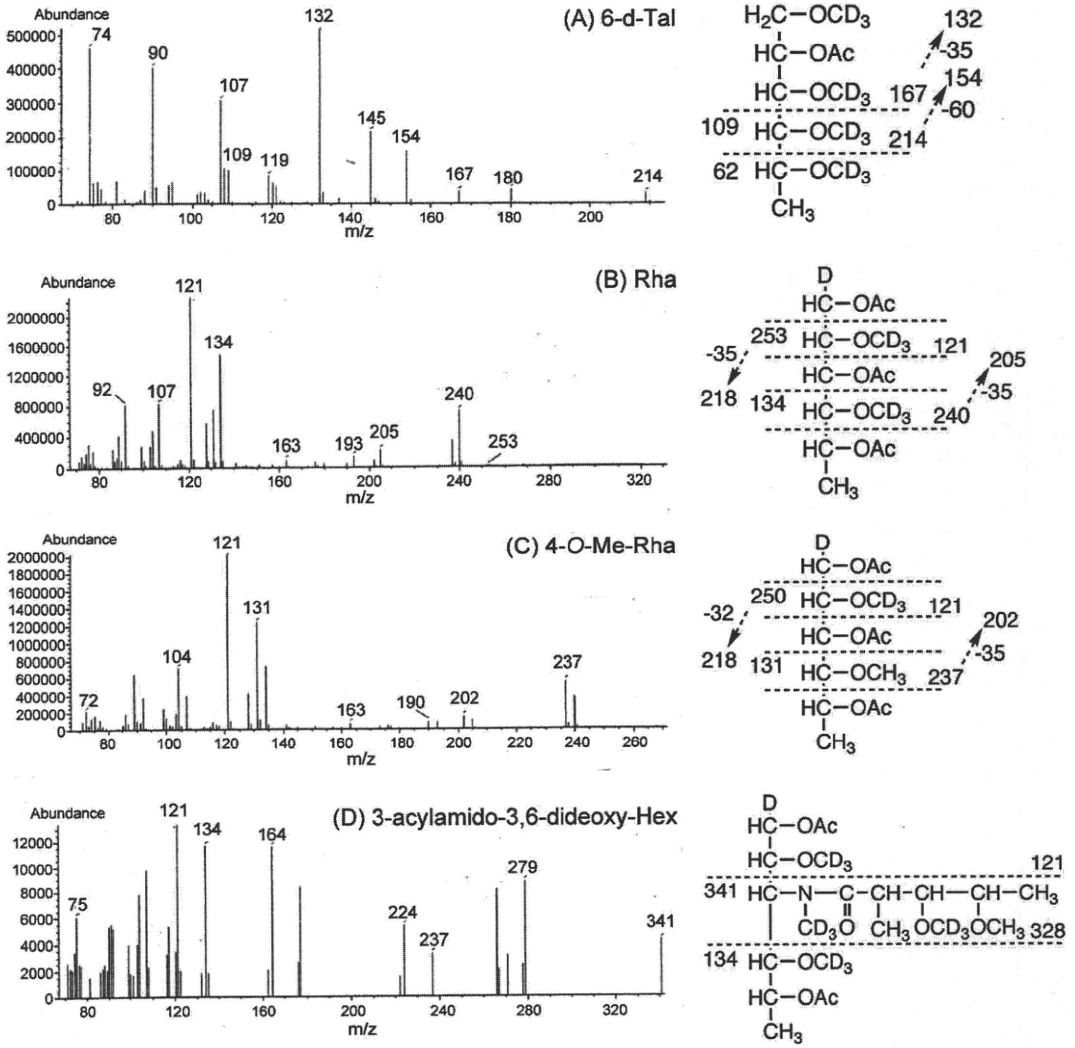

FIG. 4. GC-MS spectra of individual perdeuteromethylated alditol acetate derivatives from serotype 16 OSE. The formation of prominent fragment ions is illustrated; fragments were assigned to 1,3,4,5-tetra-*O*-deuteromethyl-2-*O*-acetyl-6-deoxy-talitol (A), 2,4-di-*O*-deuteromethyl-1,3,5-tri-*O*-acetyl-rhamnitol (B), 2-*O*-deuteromethyl-4-*O*-methyl-1,3,5-tri-*O*-acetyl-rhamnitol (C), and 2,4-di-*O*-deuteromethyl-1,5-di-*O*-acetyl-3-2′-methyl-3′-*O*-deuteromethyl-4′-methoxy-pentanoyl-deuteromethylamido-3,6-dideoxy-hexitol (D).

type 16 ATCC 13950^T was deposited in the NCBI GenBank database (accession no. AB355138). The similarity to protein sequences of each ORF is summarized in Table 1, and the genetic map for the serotype 16 GPL biosynthetic cluster was compared with those of serotype 2, 4, and 7 GPLs (Fig. 7). The *gtfB* and *drrC* genes of *M. intracellulare* serotype 16 ATCC 13950^T had 99.8% and 83.7% DNA identities with those of *M. intracellulare* serotype 7 ATCC 35847, respectively. In the DNA region between *gtfB* and *drrC* (20.8 kb), 17 ORFs were observed. Four ORFs (ORF 1, 2, 16, and 17) were homologous to those found in the same region of serotype 7-specific DNA, and the others were unique to the serotype 16 strain. No insertion of insertion elements or transposons was detected in this region. The nucleotide sequences of the ORF 1 and ORF 2 in serotype 16 strain ATCC 13950^T were homologous to those of ORF 1 and ORF 8 in serotype 7, respectively, suggesting that these two ORFs have the same function. The similarity of the deduced amino acid sequences suggested the possibility that the functions of ORF 3 and ORF 6 are to encode methyltransferase and aminotransferase, respectively. The deduced amino acid sequences of ORF 4 and ORF 5 showed significant similarities to the WxcM protein, the function of which is not clear. Interestingly, the deduced amino acid sequences of ORF 16 and ORF 17 of serotype 16 were homologous to ORF 9 of serotype 7. ORFs 1, 16, and 17 have considerable homology to glycosyltransferases. Nine ORFs, which are possibly involved in fatty acid synthesis, were detected between ORF 7 and ORF 15. It is notable that ORF 13 had a chimeric structure. The N-terminal half of ORF 13 showed similarity to phosphate butyryl/acetyl transferases, but the C-terminal half showed similarity to short-chain reductase/dehydrogenases. These results suggest that this region of DNA is responsible for the biosynthesis of the serotype 16-specific GPL.

Expression of cosmid clone no. 253 in *M. avium* serotype 1 strain. The OSE of serotype 1 GPL was composed of α-L-Rha-

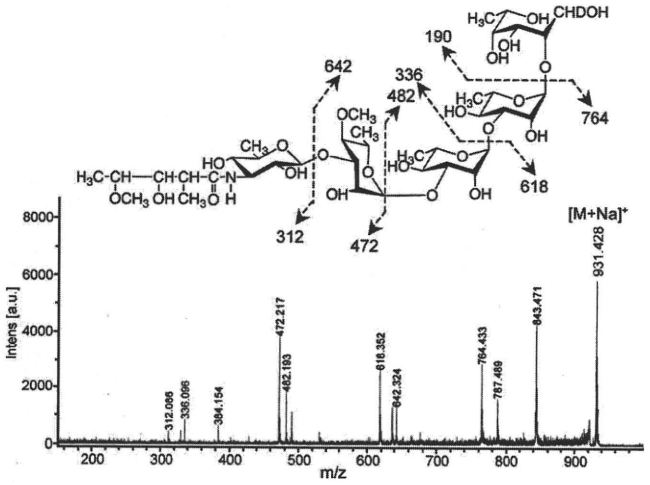

FIG. 5. MALDI-TOF/TOF MS spectrum of serotype 16 OSE. The formation of a characteristic increment in fragment ions is illustrated. The matrix was 10 mg/ml 2,5-dihydroxybenzoic acid in ethanol-water (3:7, vol/vol), and it was performed in the lift-lift mode. Intens., intensity; a.u., absorbance units.

(1→2)-6-d-L-Tal (9). The *M. avium* serotype 1 strain (NF113) was transformed with cosmid clone no. 253 containing a serotype 16-specific gene cluster and produced a new GPL with a different R_f value by TLC compared to serotype 1 GPL (Fig. 8A). The R_f value of the new GPL was identical to that of the serotype 16 GPL. The molecular weight of intact GPL, the fragment pattern of its OSE, and the GC pattern of the alditol acetate derivatives were completely equivalent to those of the serotype 16 GPL (see Fig. S2 in the supplemental material). As a result, the transformant of the serotype 1 strain expressed the cosmid clone no. 253 gene cluster and produced the serotype 16 GPL.

DISCUSSION

MAC species have serotype-specific GPLs that are characteristic components of the outer layer of the cell wall (6, 9). In addition to their serological differentiation, the chemical structures of 15 serotype-specific GPLs derived from the predominant clinical isolates have been analyzed; however, those of other GPLs remain unclear. The present study demonstrates the chemical structure of the serotype 16 GPL derived from *M. intracellulare*. We determined the glycosyl composition, linkage positions, and anomeric and ring configurations of the glycosyl residues of the serotype 16 GPL, and its OSE was defined as 3-2′-methyl-3′-hydroxy-4′-methoxy-pentanoyl-amido-3,6-dideoxy-β-Hex-(1→3)-4-*O*-methyl-α-L-Rha-(1→3)-α-L-Rha-(1→3)-α-L-Rha-(1→2)-6-d-α-L-Tal (Fig. 8B). The serotype 16 GPL should be listed as a group 2 polar GPL in the structural classification of Chatterjee and Khoo (9).

The GPLs of serotypes 7, 12, 17, and 19 have already been classified as group 2 GPLs, which are commonly composed of R→α-L-Rha-(1→3)-α-L-Rha-(1→2)-6-d-L-Tal (R, variable region), possessing a characteristic terminal sugar such as *N*-acyldeoxy-Hex. Indeed, the presence of an amido sugar has been reported in only five GPLs, serotypes 7, 12, 14, 17, and 25 (8, 9, 18). It has been determined that the OSE structure of the

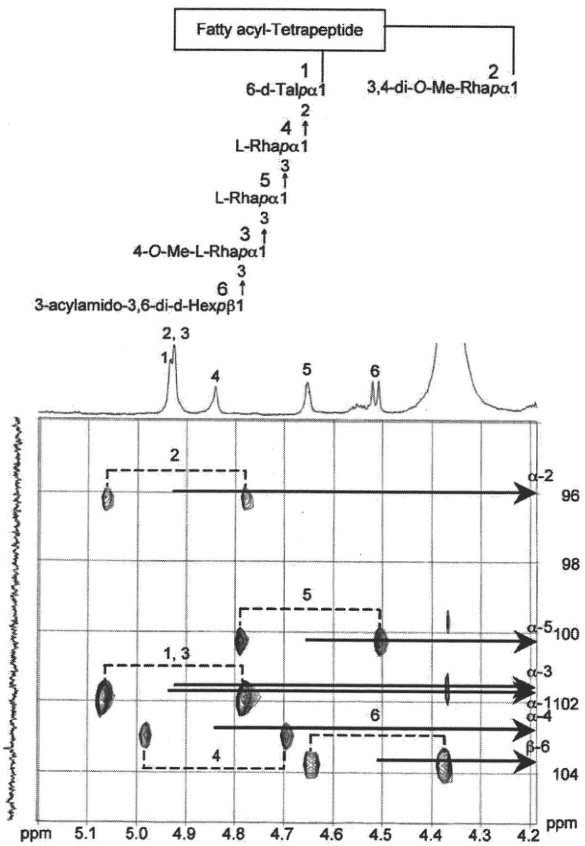

FIG. 6. Nondecoupled ^{1}H-detected [^{1}H, ^{13}C] HMQC spectrum of serotype 16 GPL. Cross-peak labels correspond to those shown on the structure.

serotype 17 GPL was 3-2′-methyl-3′-hydroxy-butanoyl-amido-3,6-dideoxy-β-D-Glc-(1→3)-4-*O*-methyl-α-L-Rha-(1→3)-α-L-Rha-(1→3)-α-L-Rha-(1→2)-6-d-L-Tal (9, 25). Based on the behavior of GPLs in TLC and the GC-MS analysis of alditol acetate derivatives, serotype 16 GPL seems to possess a unique carbohydrate epitope similar to that of serotype 17 GPL. We compared the OSE of serotype 16 GPL to that of serotype 17 GPL. The acylated amido group that was bound to the terminal sugar was different, although the linkage position was identical. Except for the terminal-acylated amido sugar, the other sugar compositions and glycosyl linkage positions were completely identical. An acylated amido group attached to the C-3 position of Hex is very unusual. To our knowledge, 3-amido-Hex is irregular in nature, although 2-amido-Hex is known to be glucosamine or galactosamine, which is frequently isolated as a component of lipopolysaccharides and glycosaminoglycans in prokaryotic and eukaryotic cells (7, 42). Further, existence of short-chain fatty acid 2-methyl-3-hydroxy-4-methoxy-pentanoic acid linked to the amido group of d-Hex is also unique. The characteristic gene cluster is thought to regulate the production of 3-acylated-amido-Hex. It is difficult to determine the species of acylated amido sugars, because no reference standard is available. The terminal sugar of the serotype 17 GPL was reviewed as a gluco-configuration, although firm evidence was not shown (9, 25). The J_{CH} and $J_{1\text{-}2}$ values for the anomeric proton in the terminal sugar were 161 and 7.7 Hz,